the plant journal

SEB SOCIETY FOR EXPERIMENTAL BIOLOGY

The Plant Journal (2024) **117**, 516–540 doi: 10.1111/tpj.16507

Natural variation in a short region of the *Acidovorax citrulli* type III-secreted effector AopW1 is associated with differences in cytotoxicity and host adaptation

Irene Jiménez-Guerrero[1], Monica Sonawane[1], Noam Eckshtain-Levi[1], Za Khai Tuang[1], Gustavo Mateus da Silva[1], Francisco Pérez-Montaño[1,2], Meirav Leibman-Markus[3], Rupali Gupta[3], Lianet Noda-Garcia[1], Maya Bar[3] and Saul Burdman[1,*]

[1]*Department of Plant Pathology and Microbiology, The Robert H. Smith Faculty of Agriculture, Food and Environment, Institute of Environmental Sciences, The Hebrew University of Jerusalem, Rehovot, Israel,*

[2]*Department of Microbiology, University of Seville, Seville, Spain, and*

[3]*Department of Plant Pathology and Weed Research, Agricultural Research Organization, The Volcani Institute, Bet Dagan, Israel*

Received 22 June 2021; revised 3 October 2023; accepted 4 October 2023; published online 21 October 2023.
*For correspondence (e-mail saul.burdman@mail.huji.ac.il).

SUMMARY

Bacterial fruit blotch, caused by *Acidovorax citrulli*, is a serious disease of melon and watermelon. The strains of the pathogen belong to two major genetic groups: group I strains are strongly associated with melon, while group II strains are more aggressive on watermelon. *A. citrulli* secretes many protein effectors to the host cell via the type III secretion system. Here we characterized AopW1, an effector that shares similarity to the actin cytoskeleton-disrupting effector HopW1 of *Pseudomonas syringae* and with effectors from other plant-pathogenic bacterial species. AopW1 has a highly variable region (HVR) within amino acid positions 147 to 192, showing 14 amino acid differences between group I and II variants. We show that group I AopW1 is more toxic to yeast and *Nicotiana benthamiana* cells than group II AopW1, having stronger actin filament disruption activity, and increased ability to induce cell death and reduce callose deposition. We further demonstrated the importance of some amino acid positions within the HVR for AopW1 cytotoxicity. Cellular analyses revealed that AopW1 also localizes to the endoplasmic reticulum, chloroplasts, and plant endosomes. We also show that overexpression of the endosome-associated protein EHD1 attenuates AopW1-induced cell death and increases defense responses. Finally, we show that sequence variation in AopW1 plays a significant role in the adaptation of group I and II strains to their preferred hosts, melon and watermelon, respectively. This study provides new insights into the HopW1 family of bacterial effectors and provides first evidence on the involvement of EHD1 in response to biotic stress.

Keywords: *Acidovorax citrulli*, bacterial fruit blotch, melon, watermelon, type III secretion, effectors, actin, endosomes, EHD1.

INTRODUCTION

Bacterial fruit blotch (BFB) of cucurbits is a devastating disease caused by the Gram-negative bacterium *Acidovorax citrulli*. Due to the impact of this disease on the cucurbit industry, and more specifically on melon and watermelon production, *A. citrulli* is considered as one of the most important plant-pathogenic species within the *Acidovorax* genus (Burdman & Walcott, 2012, 2018; Zhao & Walcott, 2018).

Acidovorax citrulli strains are divided into two major groups, I and II, that are readily distinguishable by carbon substrate utilization, whole-cell fatty acid analysis, DNA fingerprinting, and comparative genome analysis (Burdman et al., 2005; Eckshtain-Levi et al., 2016; Feng et al., 2009; Walcott et al., 2000, 2004). The two groups also differ in host preference. While group I strains have been isolated mainly from melon, but also from other non-watermelon cucurbit crops, group II strains are more strongly associated with watermelon (Burdman et al., 2005; Walcott et al., 2000, 2004). Recent experiments involving natural infection under field conditions have strengthened the differences in host preferential association between the two groups of strains (Zhao et al., 2020).

Plants utilize a defense barrier against pathogen infection via recognition of so-called pathogen-associated

molecular patterns (PAMPs). The perception process occurs through specific plant pattern recognition receptors, which results in PAMP-triggered immunity (PTI), an array of defense responses that can arrest infection of most potential pathogens (Jones & Dangl, 2006; Tang et al., 2017). Conversely, pathogenic microbes are able to deliver sets of protein effectors into the host cell to promote virulence through alteration of the host cell metabolism and suppression of host defense responses (Feng & Zhou, 2012; Macho & Zipfel, 2015). On the other hand, plants evolved to recognize some pathogen effectors, initiating a strong defense response that is named effector-triggered immunity and is often associated with a localized hypersensitive response that arrest pathogen infection (Jones & Dangl, 2006; Mansfield, 2009; Mudgett, 2005).

Like several other Gram-negative plant-pathogenic bacteria, *A. citrulli* utilizes a type III secretion system (T3SS) to deliver protein effectors (Bahar & Burdman, 2010). Eckshtain-Levi et al. (2014) carried out a comparative analysis of 11 genes encoding type III-secreted effectors (T3Es) of the group II model strain, AAC00-1. This study revealed that group I and II strains differ in their T3E arsenal. First, 3 of the 11 T3E genes of AAC00-1 were conserved in all tested group II strains, but were absent or had disrupted open reading frames (ORFs) in all tested group I strains. Second, while the other T3E genes were detected and predicted to encode functional products in both groups, most of them were highly conserved within each group but clustered separately across the two groups (Eckshtain-Levi et al., 2014). More recently, we used a multifaceted approach combining thorough sequence analysis, transcriptomics, and machine learning, that led to the identification of 58 T3E genes in the group I model strain, M6 (Jiménez-Guerrero et al., 2020). This study ranked *A. citrulli* among the richest pathogenic bacteria in terms of T3E arsenal size and confirmed the differences among group I and II strains of *A. citrulli* in their T3E cargo (Jiménez-Guerrero et al., 2020).

To date, only few studies have been reported on the role of Aop (for *Acidovorax* outer proteins) T3Es in *A. citrulli*-plant interactions. AopP was shown to suppress reactive oxygen species burst and salicylic acid content and to significantly contribute to the virulence of a group II *A. citrulli* strain in watermelon. The authors suggested that AopP suppresses plant immunity by targeting ClWRKY6 in the plant nucleus (Zhang, Yang, et al., 2020). Zhang, Zhao, et al. (2020) showed that the effector AopN locates to the cell membrane of *Nicotiana benthamiana* and induces a programmed cell death response in this plant. Recently, Fujiwara et al. (2022) suggested that Aave_4606, a T3E homologous of RipAY from *Ralstonia solanacearum*, recognizes host-specific thioredoxins, which specifically activates the Aave_4606 γ-glutamyl cyclotransferase activity, leading to a decrease in host cellular glutathione.

We are particularly interested in effector AopW1 (*Acidovorax* outer protein W1). The genes encoding this effector are *APS58_3289* in the genome of the group I model strain M6, and *Aave_1548* in the genome of the group II model strain AAC00-1 (NCBI accessions CP02973.1 and NC_008752.1, respectively). We named this effector AopW1 due to its similarity to the *Pseudomonas syringae* pv. *maculicola* T3E, HopW1. Lee et al. (2008) showed that *hopW1* expression in *P. syringae* pv. *tomato* promotes virulence in *A. thaliana* Col-0. The authors also showed that the C-terminal region of HopW1 is needed for triggering defense responses. Later, Kang et al. (2014) showed that filamentous actin (F-actin) is a major virulence target of HopW1. They showed that HopW1 interacts with and reduces actin filaments *in vitro* and *in planta*, disrupts the actin cytoskeleton, and affects actin-dependent cell biological processes that are critical for plant immunity like endocytosis and protein trafficking into vacuoles. The C-terminal region of HopW1 was also needed for these phenotypes (Kang et al., 2014).

AopW1 is strongly conserved within *A. citrulli* strains that belong to the same group, while differing between the two groups. Specifically, group I and II versions of AopW1 are 485 amino acids (a.a.) long and are highly conserved except for a hypervariable region (HVR) between a.a. positions 147 and 192, that shows 14 differences between the two versions (~30% dissimilarity) (Eckshtain-Levi et al., 2014). Traore et al. (2019) demonstrated that both group I and II AopW1 significantly contribute to the virulence of *A. citrulli* in melon and watermelon, respectively. Interestingly, in *N. tabacum*, group I AopW1 triggered a stronger cell death than that exerted by group II AopW1, suggesting that the differences in the HVR between the two versions correlate with molecular function (Traore et al., 2019). Recently, we showed that *aopW1* expression in *A. citrulli* M6 is regulated by the T3SS transcriptional activator HrpX, and validated that AopW1 is translocated to the plant cell in a T3SS-dependent manner (Jiménez-Guerrero et al., 2020).

In the present study, we investigated the sequence-function relationship of AopW1. We asked whether differences in the HVR between group I and II AopW1 are determinants of their functional performance, including cytotoxicity, actin filament disruption ability, interaction with plant cell compartments, and ability to induce plant cell death and reduce callose deposition. Overall, our findings demonstrate that the group I version of AopW1 has increased toxicity as compared to group II AopW1. We also identified amino-acid residues in the HVR region that are critical for the activity of AopW1, and probably of effectors belonging to the HopW1 family. Further, we found that the endosome-associated protein EHD1 significantly attenuates AopW1-induced cytotoxicity. Last, inoculation assays with melon and watermelon plants involving group I and II wild-type strains, as well as *aopW1* mutants and

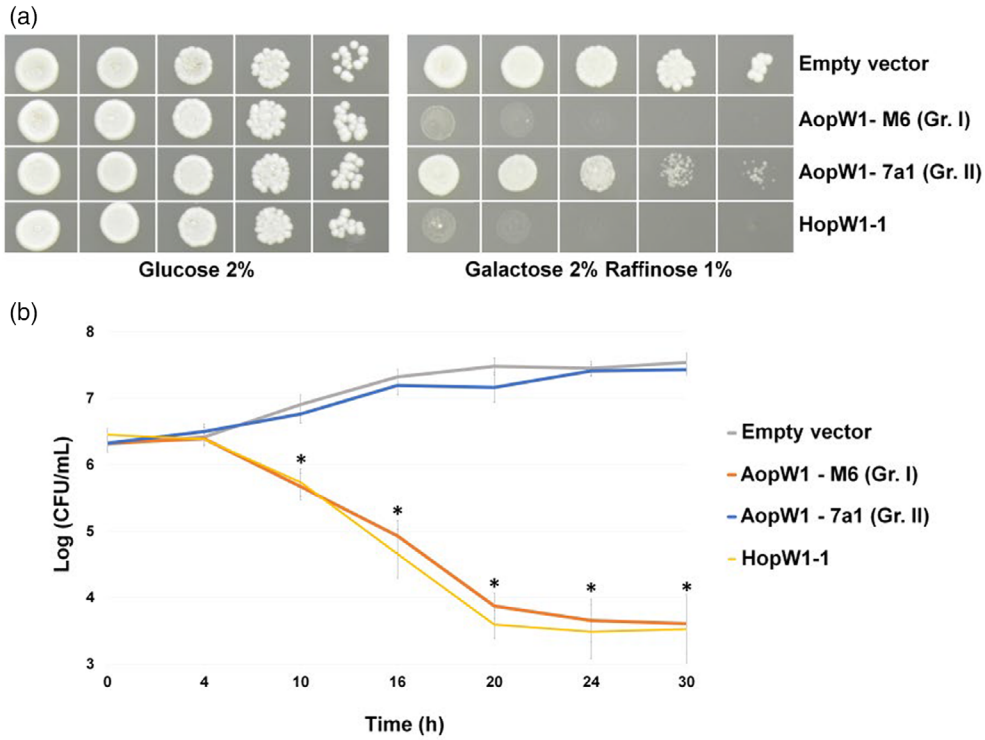

Figure 1. *Acidovorax citrulli* group I AopW1 is more toxic than group II AopW1 to yeast cells.
(a) Yeast growth inhibition assays. The open reading frames (ORFs) of *aopW1* from *A. citrulli* strains M6 (group I) and 7a1 (group II), and *hopW1* from *Pseudomonas syringae* pv. *maculicola* ES4326 were cloned into pGML10 under the control of a galactose inducible promoter. The plasmids were transformed into *Saccharomyces cerevisiae* BY4741. Serial dilutions (10^0 to 10^{-4}; from left to right) of the yeast cultures were spotted on glucose (repressing) or galactose/raffinose (inducing) media. Controls were yeast cells carrying pGML10 (empty vector). Pictures were taken after 3 days of growth at 28°C and are representative of three independent experiments.
(b) Cell viability assays of yeast expressing the aforementioned effectors. Yeast cells were grown in an inducing medium, collected at different time points, serially diluted, and spotted ona to repressing medium to assess the number of viable cells. Data represent means and standard errors (SE) from one experiment out of three with similar results (with four replicates per treatment and time point). Asterisks indicate significant ($P < 0.05$) differences compared to the empty vector at each time point by Student's *t*-test.

complemented strains, revealed this T3E plays a key role in determination of host preferential association in *A. citrulli*.

RESULTS

Heterologous expression in yeast reveals differences in cytotoxicity between group I and II versions of AopW1

To assess differences in cytotoxicity between group I and II AopW1, we used a yeast-based heterologous system that has been used to detect phenotypes of bacterial effectors (Salomon & Sessa, 2010; Siggers & Lesser, 2008). The *aopW1* ORFs of strains M6 and 7a1 (belonging to groups I and II, respectively) were cloned into the yeast expression vector pGML10 and transferred to *Saccharomyces cerevisiae* BY4741 for heterologous expression. It is worth mentioning that the 7a1 *aopW1* ORF is 100% identical to that of the group II model strain AAC00-1 (Eckshtain-Levi et al., 2014).

Growth inhibition assays were carried out in inducing media (supplemented with 2% galactose and 1% raffinose), under regular conditions or with the addition of stressing compounds. It has been shown that combination of different stressors may increase yeast sensitivity thus aiding to detect effector-induced phenotypes (Salomon et al., 2011; Salomon et al., 2012; Siggers & Lesser, 2008). As stressors, we used 7 mM caffeine, 0.5 M sodium chloride, or 1 M sorbitol (Kuranda et al., 2006; Salomon et al., 2011; Yoon et al., 2003). Controls were yeast plated on repressing media (supplemented with 2% glucose).

Under regular conditions, group I AopW1 (AopW1-M6) exerted strong growth inhibition of yeast cells, while the group II version (AopW1-7a1) had a very slight effect (Figure 1a). The growth inhibition effect exerted by group I AopW1 was comparable to that induced by *P. syringae* HopW1 and slightly higher than that exerted by the HopW1-homologous effector from *Xanthomonas translucens* (Figure 1a; Table S1). Growth inhibition by group I AopW1 was increased when combined with NaCl, while the growth inhibition effect of group II AopW1 was increased in combination with caffeine, NaCl, or sorbitol, though at substantially lower levels than the effects exerted by group I AopW1 (Table S1).

To assess whether yeast growth inhibition was due to cell death or growth arrest, we carried out yeast cell viability time curves. A significant decrease ($P < 0.05$) of viable cells was detected in yeast-expressing group I AopW1, in a similar manner as observed for the expression of *P. syringae* HopW1. In contrast, the viability of cells expressing group II AopW1 did not significantly differ from controls carrying empty pGML10, demonstrating that group II AopW1 does not exert a strong toxic effect on yeast (Figure 1b). AopW1 expression in yeast under inducing conditions was confirmed by Western blot analysis. Remarkably, detection of group I AopW1 was extremely difficult (Figure S1a), presumably due to its strong toxic effect on yeast.

Group I AopW1 strongly affects yeast F-actin organization *in vivo* and disrupts non-muscle F-actin *in vitro*

Actin is a highly abundant and conserved protein that is essential for the survival of most eukaryotic cells. It occurs in a globular monomeric (G-actin) stage or in a filamentous polymeric (F-actin) form (Pollard, 2016; Pollard et al., 2000). The actin cytoskeleton is a complex network of dynamic polymers, which has an important role in a wide range of cellular processes (Mishra et al., 2014; Pollard & Borisy, 2003). As aforementioned, Kang et al. (2014) showed that *P. syringae* HopW1 disrupts the actin cytoskeleton.

To assess the effects of AopW1 in yeast cells, budding yeast cultures were stained with the actin stain TRITC-phalloidin 8 h after expression of group I or II AopW1. During budding, the actin filament network of yeast cells presents three specific structures: cortical actin patches, actin cables, and the actomyosin ring (Mishra et al., 2014; Figure S2a). Yeast cells carrying empty pGML10 displayed normal formation of actin filaments and migration of actin patches to the daughter cells, and a similar picture was observed in cells expressing group II AopW1. In contrast, cells expressing group I AopW1 exhibited a strong disorganization of the actin structures, with actin patches seeming disorganized through the cell (Figure S2b). In yeast cells expressing group I AopW1 we detected less formation of daughter cells than in the two other treatments (Figure S2c).

To assess whether the effect caused by group I AopW1 is due to actin depolymerization activity, we carried out *in vitro* sedimentation assays with pre-assembled non-muscle F-actin. In these assays, we used purified recombinant AopW1 from group I and II strains without the first 100 a.a. of their N-terminus (AopW1-M6$_{101–485}$ and AopW1-7a1$_{101–485}$, respectively) fused to a poly-histidine (His) tag in both extremes. The N-terminal part of AopW1 was not included because we were not able to express sufficient amounts of soluble full-length AopW1. As shown in continuation, the N-terminal 100 a.a. of this effector is not needed for cytotoxic activity in yeast. Expression and purification of the recombinant proteins were verified by sodium dodecyl sulfate-polyacrylamide gel electrophoresis (SDS-PAGE) and Western blot analysis (Figure 2a,b). Incubation of pre-assembled non-muscle F-actin with poly-His-AopW1-M6$_{101–485}$, but not with α-actinin (which binds to F-actin) or bovine serum albumin (BSA; which does not bind to F-actin), led to a reduction of about 22% of F-actin (pellet fraction; P), with a concomitant increase of about 34% of G-actin (supernatant fraction; S), relative to control treatment (F-actin alone) (Figure 2c). Recombinant group II AopW1 (poly-His-AopW1-7a1$_{101–485}$) was able to induce actin depolymerization but at substantially lower levels than the group I version (Figure 2c). The presence of both recombinant variants of AopW1 was validated by Western blot analysis (Figure 2d).

Combined substitutions of specific amino acid residues in AopW1 alter cytotoxicity in yeast

T3Es sharing similarity with AopW1 occur in other plant-pathogenic bacteria. In addition to the aforementioned HopW1 from *P. syringae* and homologous effectors from *X. transluscens*, AopW1 homologs occur in other *Pseudomonas* spp., in *Erwinia mallotivora* and in other plant-pathogenic *Acidovorax* species (Figure 3a). As said above,

Figure 2. AopW1 disrupts F-actin *in vitro*.
(a) Expression of recombinant, His-tagged AopW1$_{101–485}$ from strains M6 (group I) and 7a1 (group II) in *Escherichia coli* BL21(DE3) at 0, 1, 2 and 4 h after induction by 1 mM isopropyl β-D-1-thiogalactopyranoside (IPTG).
(b) Purification of AopW1$_{101–485}$ from strains M6 and 7a1 4 h after induction by 1 mM IPTG. Lines 1 and 2 show purified AopW1$_{101–485}$ from M6 and 7a1, respectively. In (a, b), upper panels show Coomassie blue staining [black arrow in (a) indicates AopW1$_{101–485}$], and bottom panels show immunodetection of AopW1$_{101–485}$ using an anti-His primary antibody.
(c) *In vitro* F-actin disruption assays. Preassembled F-actin (filamentous polymer) was incubated with 0.35 μM of AopW1$_{101–485}$ from strains M6 (group I) or 7a1 (group II), 2 μM α-actinin or 2 μM BSA for 1.5 h at 24°C and centrifuged at 150 000 ***g*** for 1.5 h. Samples were partitioned into supernatant (S) and pellet (P) fractions to separate G-actin (globular subunit) and F-actin, respectively. Proteins were separated by SDS-PAGE and stained with Coomassie blue. α-actinin was used as positive control for actin binding activity (presence in S or P when α-actinin was incubated alone or with F-actin, respectively), and as negative control for actin disruption activity (F-actin remained polymerized in P). BSA was used as negative control for actin binding and actin disrupting activities (presence in S when BSA was incubated with F-actin; F-actin remained polymerized in P). Quantification (%) of actin change in S and P relative to control (F-actin alone) was done by ImageJ and is indicated in parentheses.
(d) His-tagged group I (M6) and group II (7a1) AopW1$_{101–485}$ were detected in the supernatant (S) by Coomassie blue staining (upper panel) and Western blot using anti-His primary antibodies (bottom panels). Immunodetection was done in samples containing 0.35 μM AopW1$_{101–485}$ without the presence of F-actin (anti-His antibodies reacted unselectively with F-actin, independently of the presence or absence of AopW1$_{101–485}$; not shown). Marker molecular masses (kDa) are shown in the left. The experiment was performed twice with similar results.

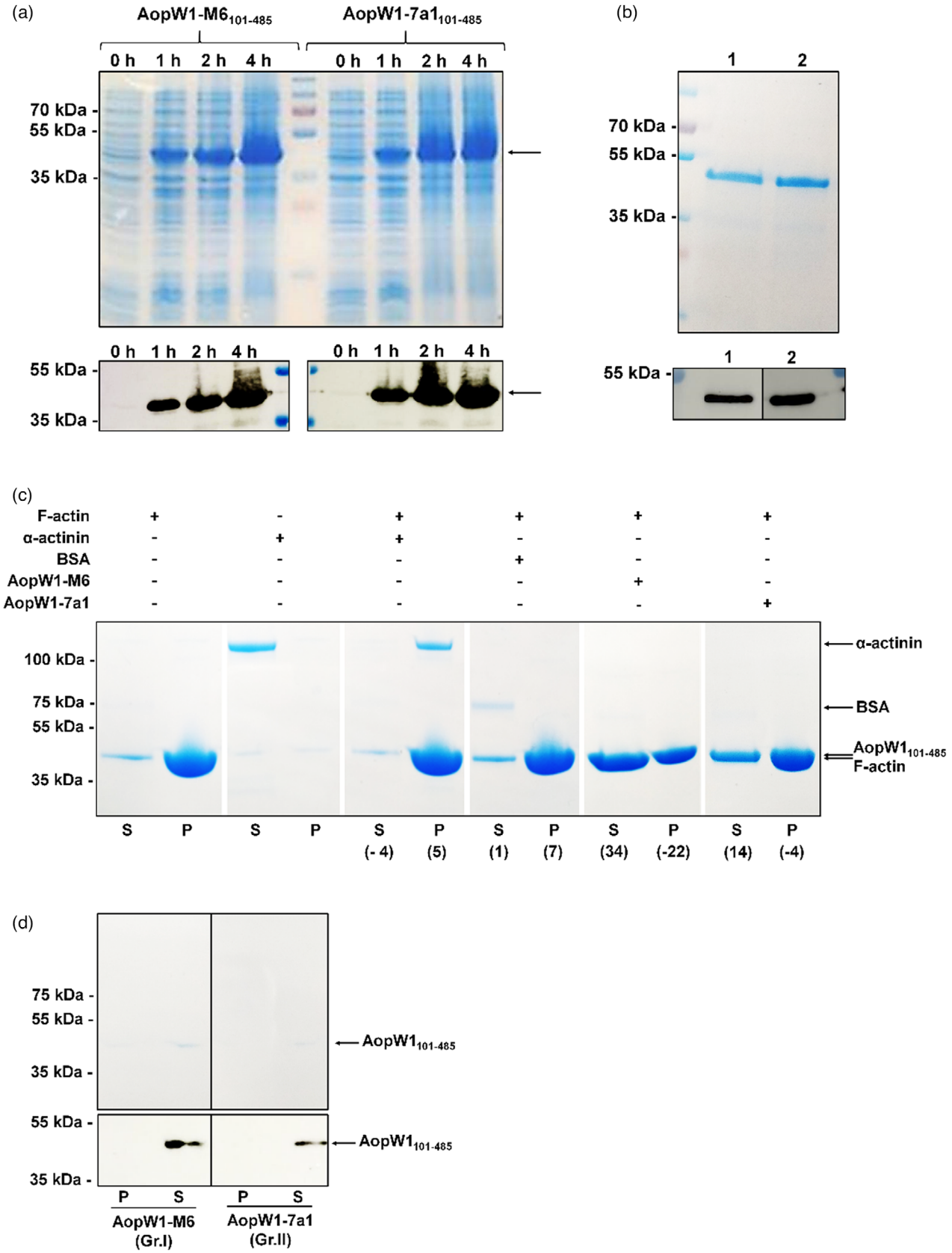

the *aopW1* gene is highly conserved among group I and II strains of *A. citrulli*, except for a 138-bp HVR located at nucleotide positions 439–576 (a.a. positions 147–192 in the encoded products). Of the 46 a.a. included in the HVR, 14 are different between the group I and II versions of the effector (Figure 3b). Although group I and II AopW1 share high levels of identity as compared with homologs from other bacteria, including in the HVR (Figure 3b), of the 14 positions that distinguish between them, 6 are strongly conserved between group I AopW1 and the homologous T3Es from *Pseudomonas*, *Xanthomonas*, and *Erwinia* species. These are a.a. positions 154, 162, 167, 174, 177, and 189 (named positions 1–6, respectively, as indicated in the bottom of Figure 3b). Intriguingly, variation in the HVR also occurs among strains of *A. avenae*, with some variants resembling group I AopW1 and others resembling group II AopW1 (Figure 3b).

We hypothesized that differences in the HVR, and particularly in the aforementioned six positions, are important determinants of the different patterns of cytotoxicity between group I and II versions of AopW1. In this regard, it is worth mentioning that the AopW1 HVR aligns with part of the C-terminal region of *P. syringae* HopW1, which is required for actin cytoskeleton disruption (Kang et al., 2014).

To assess the importance of these six positions for AopW1 activity, we generated several constructs in which the group I and II *aopW1* ORFs were altered by site-directed mutagenesis to substitute each of these residues by the a.a. present in the other version (Tables S2 and S3). We also generated group I and II AopW1 variants carrying multiple substitutions (Table S3). All constructs were tested in yeast growth inhibition assays. Expression of the mutated variants of AopW1 in inducing medium was confirmed by Western blot analyses. While immunodetection of group II AopW1-derived variants was easy (Figure S1b, c), immunodetection of most mutated variants of group I AopW1 was difficult yielding very weak bands (Figure S1a), presumably because of their stronger toxicity as compared with group II variants.

Most individual substitutions in the HVR did not lead to significant alterations in yeast growth inhibition ability in comparison with the corresponding wild-type versions (Figure S3). The only exception was the AopW1 group II variant carrying an individual substitution in position 6 (M-189-T) that reduced cytotoxicity to the empty vector level (Figure S3b). Besides the HVR, group I and II AopW1 differ in position 319 (leucine in group I; serine in group II). Swap substitutions in this position (L319S and S319L in group I and II AopW1, respectively; Table S2) did not alter yeast growth inhibition ability as compared with the corresponding wild-type versions (Figure S4).

Characterization of combined substitutions in the background of group I AopW1 showed that only one variant, carrying three substitutions [1 (V-154-I) + 2 (R-162-Q) + 3 (P-167-A); hereafter group I (1+2+3) AopW1], had significantly reduced cytotoxicity as compared with the wild-type version of the effector (Figure 4a). Surprisingly, adding substitutions in positions 4 (A-174-T) and/or 6 (T-189-M) to this variant, abolished this effect, namely, led to a growth inhibition effect that was similar to that of group I AopW1 (Figure 4a).

In the case of group II AopW1, a variant carrying substitutions in positions 1 to 4 [1 (I-154-V) + 2 (Q-162-R) + 3 (A-167-P) + 4 (T-174-A); hereafter group II (1+2+3+4) AopW1], had a substantially higher yeast growth inhibition ability as compared with the group II wild-type version (Figure 4b). However, adding a fifth substitution to this variant [6 (M-189-T)] abolished this effect. In addition, a combination of two substitutions [1 (I-154-V) + 2 (Q-162-R)] and a combination of three substitutions [1 (I-154-V) + 2 (Q-162-R) + 3 (A-167-P)] led to a subtle increment in the growth inhibition effect as compared with the group II wild-type version of AopW1 (Figure 4b).

Overall, results from these experiments demonstrated that the AopW1 HVR is important for the induction of cytotoxicity in yeast. These experiments also validated the importance of the six positions that are conserved between group I AopW1 and most homologous effectors from other plant-pathogenic bacteria. However, it appears that the interactions among these positions are complex and not merely additive.

The HVR and the C-terminal part of AopW1 are required for cytotoxic activity

To learn about the importance of the different parts of AopW1 for its activity, we generated pGML10 constructs carrying several N- and C-terminal truncated variants in the background of group I AopW1 (Table S2; Figure 5). Growth inhibition assays revealed that the N-terminal part of the effector (first 135 residues; AopW1-M6$_{\Delta 1–135}$) is not

Figure 3. Comparison of AopW1 and homologous effectors.
(a) AopW1 protein-based phylogeny from *Acidovorax*, *Pseudomonas*, *Xanthomonas*, and *Erwinia* species. Sequences were aligned using MUSCLE and the phylogeny was reconstructed using maximum likelihood methods included in the SeaView program (ref: PMID 19854763). Numbers at nodes are the approximate likelihood ratio test supporting each branch. The scale bar shows amino acid (a.a.) substitutions per site.
(b) Alignment of the hypervariable region (HVR) of *A. citrulli* AopW1 from group I and group II strains with corresponding regions from homologous effectors. The alignment corresponds to a.a. positions 147–192 of AopW1, and it was done using ClustalW. Black asterisks indicate the 14 a.a. differences between group I and II AopW1 in this region. Blue asterisks indicate the strongly conserved positions within *Acidovorax* spp., which differ in other species. Gray shading and numbers at the bottom of the alignment indicate the six conserved a.a. positions between group I AopW1 and homologous effectors from other species.

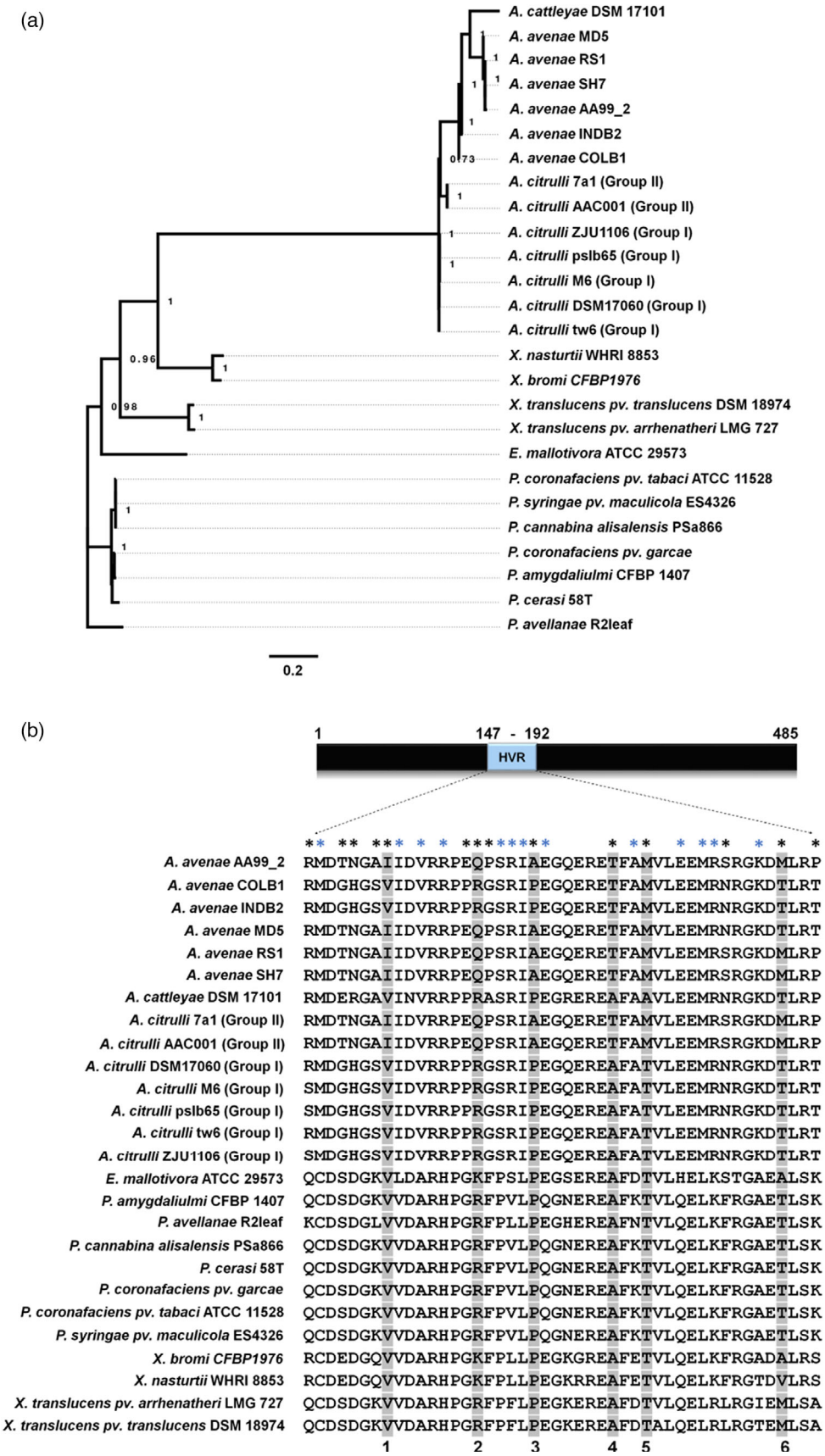

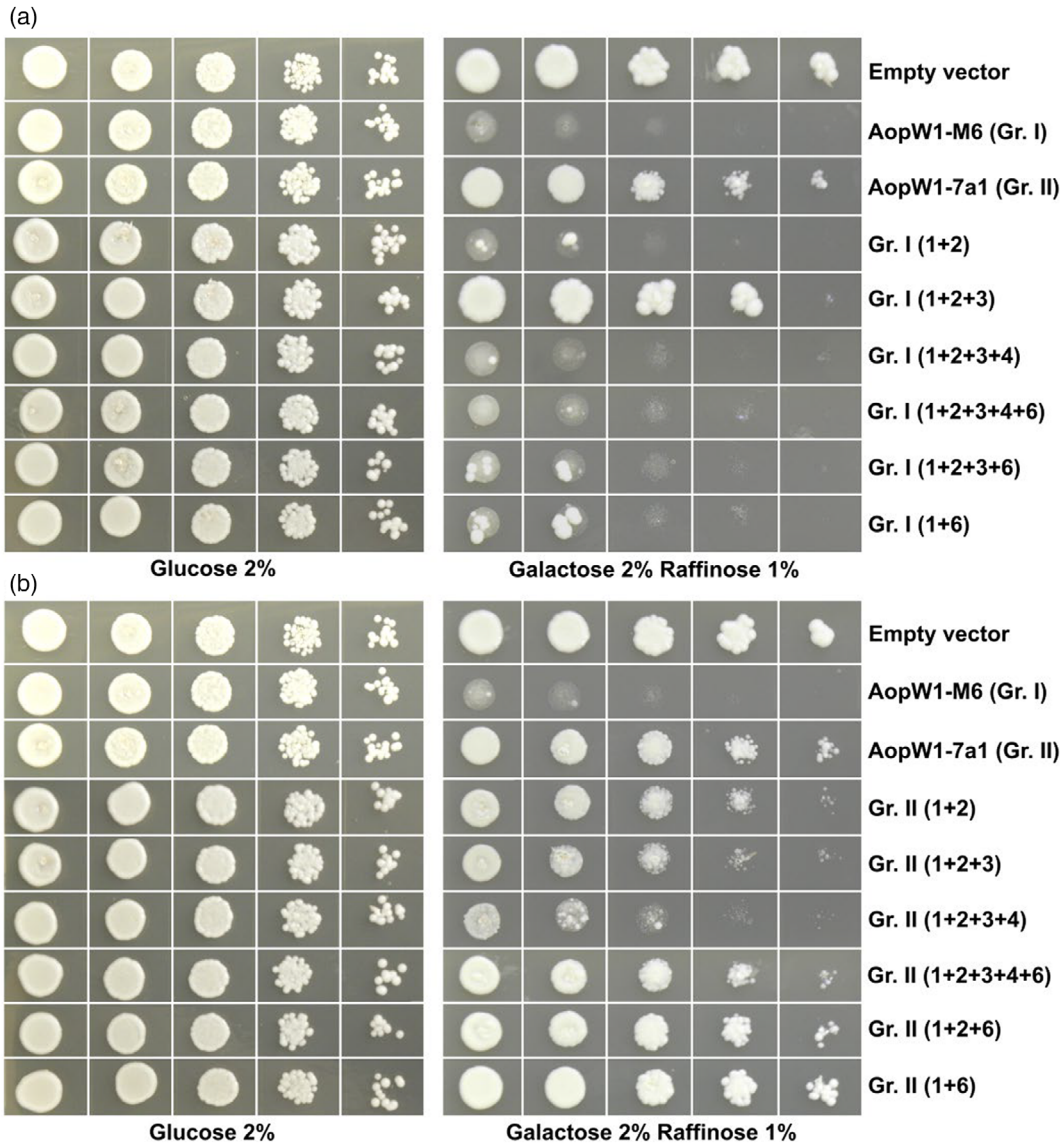

Figure 4. Effects of combined amino acid substitutions in the AopW1 highly variable region (HVR) on yeast growth inhibition.
Yeast growth inhibition assays of different variants of group I (a) and group II AopW1 (b) carrying several combinations of a.a. substitutions in the six positions that are conserved among group I AopW1 and homologous effectors from other bacterial species (see Figure 3; Table S3 for variant details). Serial dilutions (10^0 to 10^{-4}; from left to right) of *Saccharomyces cerevisiae* BY4741 carrying the ORF of the *aopW1* variants in pGML10 were spotted on glucose (repressing) and galactose/raffinose (inducing) medium. Pictures were taken after 3 days of growth at 28°C and are representative of three independent experiments.

important for yeast inhibition ability. However, the removal of the next 10 residues (AopW1-M6$_{\Delta 1-145}$) significantly reduced this ability. Further removal of 30 residues (AopW1-M6$_{\Delta 1-175}$), which also removed part of the HVR, almost abolished yeast growth inhibition ability of AopW1. The C-terminal part was found to be critical for the cytotoxic ability of AopW1. While removal of the last 10 residues (AopW1-M6$_{\Delta 476-485}$) did not affect AopW1 activity, removal of the last 25 residues (AopW1-M6$_{\Delta 461-485}$) completely abolished it (Figure 5). These experiments revealed that the crucial sequence for cytotoxicity of group I AopW1 ranges from position 135 to 475.

Conserved residues in the AopW1 HVR are crucial for induction of cell death in *N. benthamiana*

Traore et al. (2019) showed that transient expression of group I and II AopW1 induces a water-soaking-like cell death phenotype in *N. benthamiana* leaves. Here we assessed the effects exerted by selected group I and II AopW1 variants carrying substitutions in some of the HVR a.a. positions (selected based on results from yeast inhibition assays). The ORFs of the AopW1 variants were cloned into the Gateway-compatible plant transformation vector pEarleyGate 101 (Table S2) and agroinfiltrated into *N.*

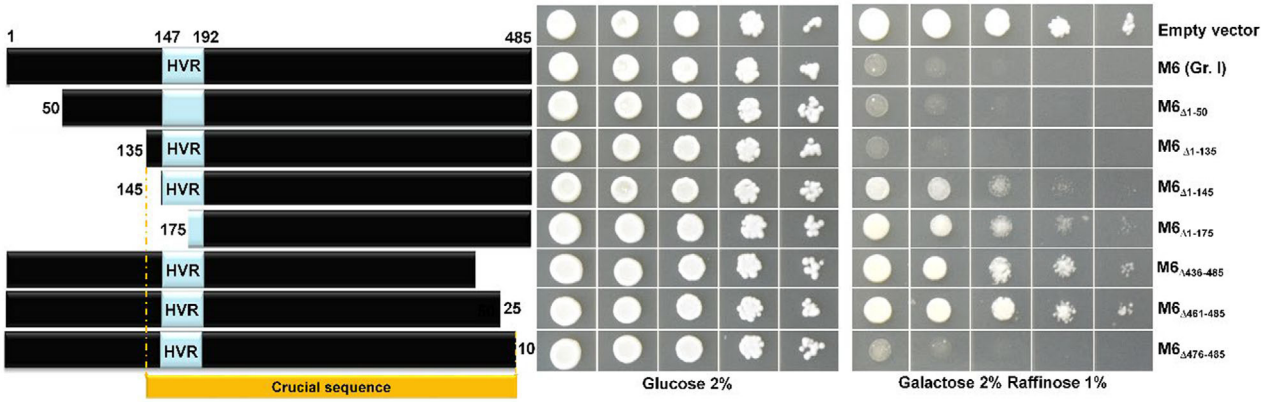

Figure 5. The highly variable region (HVR) and the central and C-terminal regions of AopW1 are required for cytotoxicity.
Wild-type and shortened variants of *Acidovorax citrulli* M6 (group I) *aopW1* were cloned in pGML10 and transformed into *Saccharomyces cerevisiae* BY4741 for growth inhibition assays. Serial dilutions (10^0 to 10^{-4}; from left to right) of the different yeast strains were spotted on glucose (repressing) and galactose/raffinose (inducing) medium. Pictures were taken after 3 days of growth at 28°C and are representative of three independent experiments.

benthamiana leaves. Their expression was verified by Western blot analysis (Figure S5).

In line with the results reported by Traore et al. (2019), both groups I and II AopW1 were toxic to *N. benthamiana* leaves, with group I AopW1 inducing a much stronger cytotoxic effect. Differences between the two AopW1 versions were observed by the naked eye (Figure 6A,B) and were confirmed by quantitative measurements that showed significantly higher induction of cell death (Figure 6C) and ion leakage (Figure 6E) by group I AopW1 as compared with group II AopW1. The group I variant of AopW1 carrying the three HVR substitutions that reduced cytotoxicity in yeast [group I (1+2+3) AopW1] induced slightly but significantly lower cell death and ion leakage than group I AopW1. Also in agreement with yeast growth inhibition assays, expression of the group II variant of AopW1 carrying the four substitutions that increased cytotoxicity of this effector in yeast [group II (1+2+3+4) AopW1] induced significantly higher cell death and ion leakage in *N. benthamiana* leaves as compared with group II AopW1 (Figure 6C,E). These results demonstrate the importance of the HVR and of the above a.a. positions for *in planta* cytotoxicity of AopW1.

AopW1 localizes to the plant cell cytoplasm and interacts with chloroplasts

The subcellular localization of AopW1 was studied by confocal microscopy following agroinfiltration of *N. benthamiana* leaves with *Agrobacterium tumefaciens* carrying AopW1 ORFs fused to yellow fluorescent protein (YFP) in plasmid pEarleyGate 101 (Table S2). Overall, experiments with group II AopW1 were easier than with group I AopW1, due to the extensive cell death caused in *N. benthamiana* infiltrated sites by the latter, which challenged the analysis.

Both group I and II AopW1 were located in the cytoplasm, with no nuclear localization being detected (Figure 7a,b). Interestingly, both effectors co-localized with chloroplasts. This was more clearly detected for group II AopW1 (Figure 7b), probably because of the aforementioned extensive damage caused by group I AopW1 to *N. benthamiana* cells. Co-localization of AopW1 with chloroplasts was in agreement with the detection of a chloroplast transit peptide (cTP) in the N-terminus of the effector, as detected by ChloroP 1.1 (Emanuelsson et al., 1999), WoLF PSORT (Horton et al., 2007) and Localizer (Sperschneider et al., 2017) software (Appendix S1). Indeed, the deletion of the first N-terminal 85 residues from group II AopW1, which contains the cTP sequence, abolished the co-localization of AopW1 with chloroplasts (Figure 7c). Similar co-localization with chloroplawaswere detected for the group I (1+2+3) and group II (1+2+3+4) variants of AopW1 (Figures S7 and S8, respectively).

Group I AopW1 severely disrupts the plant actin cytoskeleton and affects endoplasmic reticulum organization

To evaluate the interaction of AopW1 with the plant actin cytoskeleton, we co-expressed YFP-fused AopW1 with the plant actin marker, DsRed-ABD2 (Voigt, Timmers, Šamaj, Hlavacka, et al., 2005). While both group I and II AopW1 co-localized with the actin marker, only group I AopW1 disrupted the actin cytoskeleton (Figure 8a). The mutated version of group I, group I (1+2+3) AopW1, was still able to disrupt actin, though to a lesser extent than group I AopW1 (Figure S6), while the mutated version of group II, group II (1+2+3+4), appeared to disrupt actin to a greater degree than group II AopW1 (Figure S7).

Proteins involved in actin polymerization are often associated with the endoplasmic reticulum (ER) (Zhang

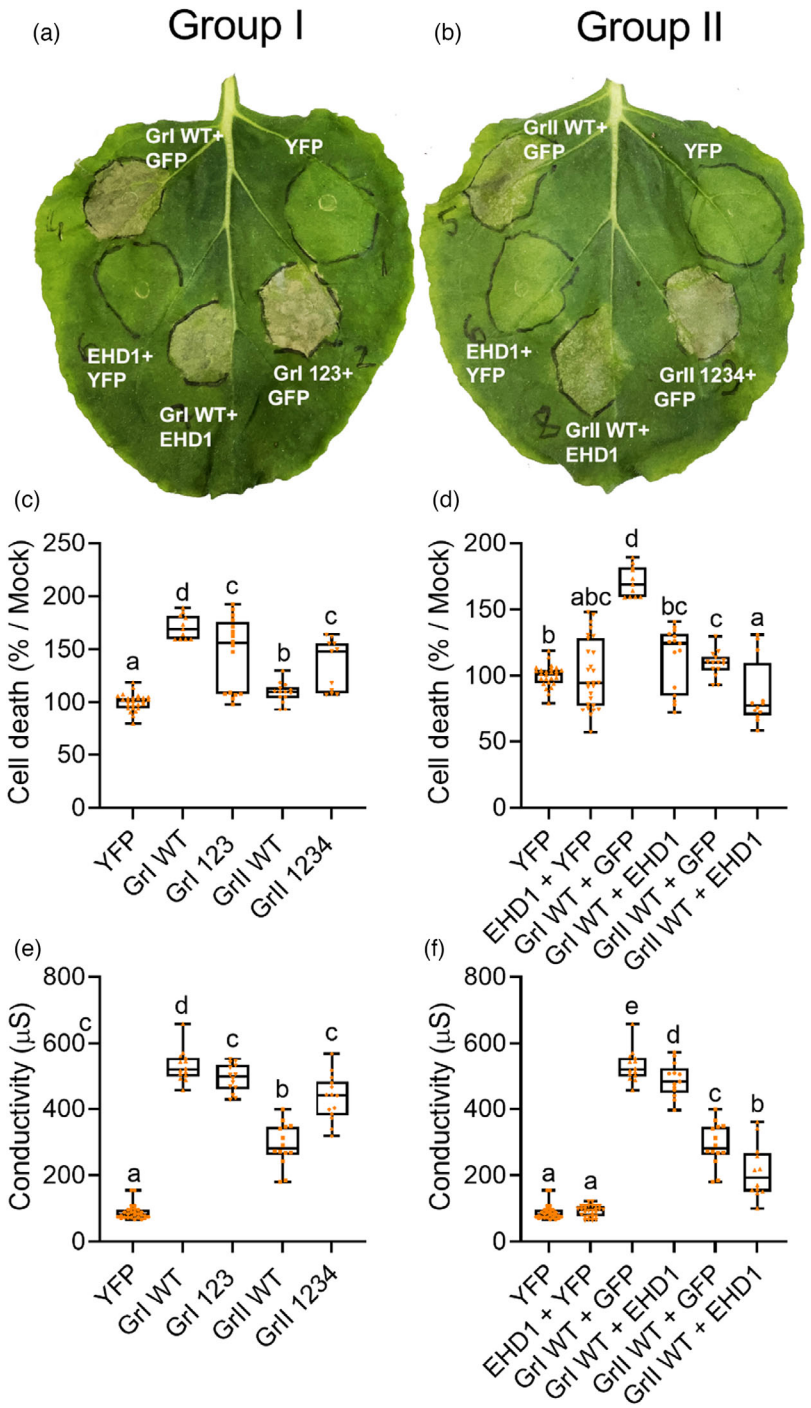

Figure 6. Transient expression of AopW1 in *Nicotiana benthamiana* leaves.
Wild-type and mutated variants of *Acidovorax citrulli* M6 (group I) AopW1 (A) and 7a1 (group II) AopW1 (B) were transiently expressed in *N. benthamiana* leaves following in combination with the endosome-associated protein EHD1 (*Agrobacterium tumefaciens* carrying pBIN19-*Pro35S*:AtEHD1-GFP) or with GFP as control (*A. tumefaciens* carrying pBIN19-*Pro35S*:free-GFP) (Table S2). GrI WT and GrII WT are the group I and II wild-type versions of AopW1, respectively. GrI 123 and GrII 1234 are the group I (1+2+3) and II (1+2+3+4) AopW1 variants of the effector modified in selected a.a. positions, respectively (Table S3). Controls without agroinfiltration of AopW1 variants included infiltration with *A. tumefaciens* carrying pEarleyGate 101 containing free-YFP (YFP; Table S2), alone or in combination with EHD1. Pictures were taken 3 days after agroinfiltration.
Cell death (C, D) was quantified 3 days after agroinfiltration (12 leaves infiltrated in four separate experiments).
Conductivity (E, F) was measured 18 h after agroinfiltration (14 samples generated from nine plants). Boxplots represent minimum to maximum values with inner quartile ranges (box), outer quartile ranges (whiskers), and median (line in box), all values shown. Different letters indicate statistically significant differences among samples based on Mann–Whitney test for (C) ($P < 0.018$) and (D) ($P < 0.028$), and Kruskal Wallis one-way analysis of variance (ANOVA) for (E) ($P < 0.003$) and (F) ($P < 0.04$).

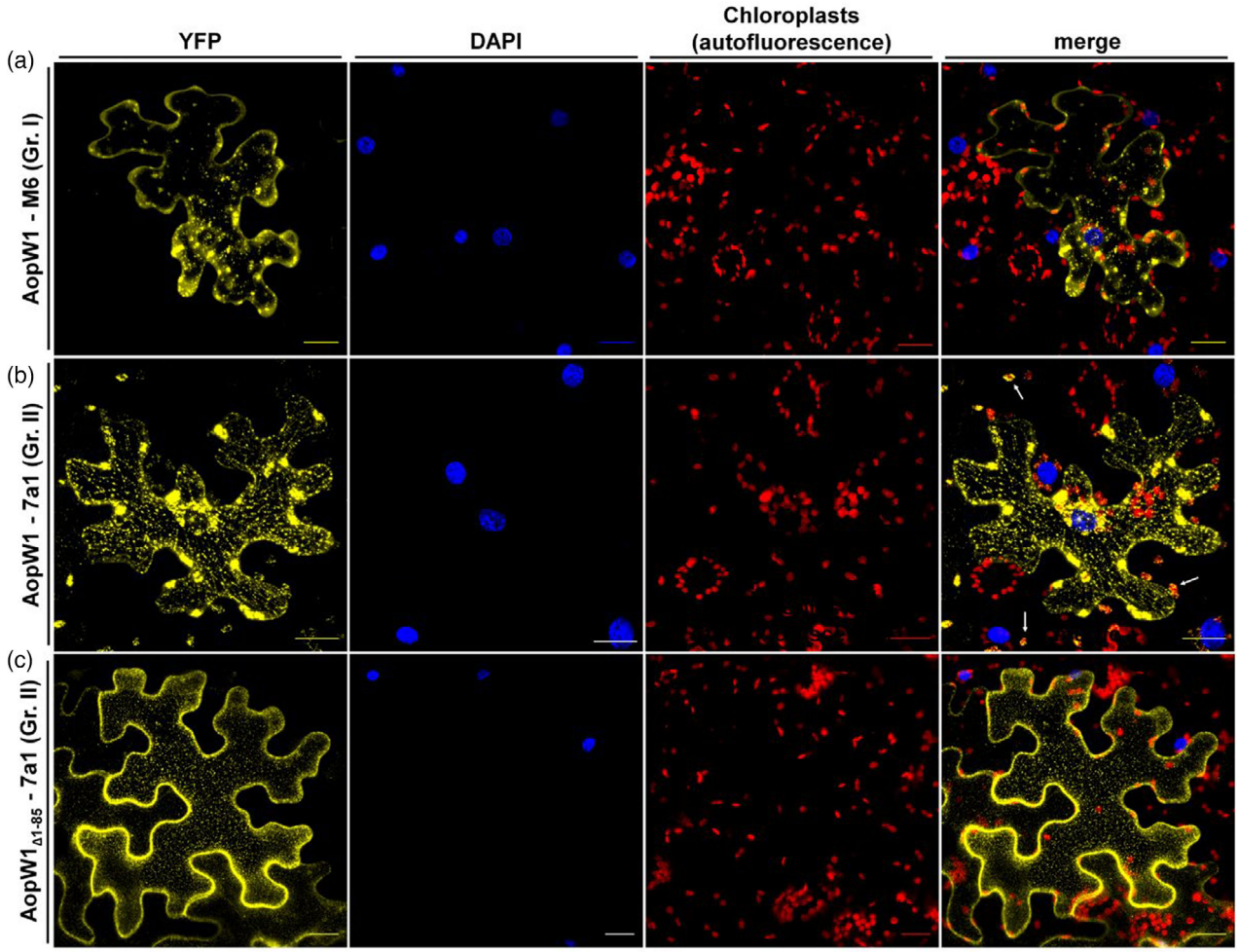

Figure 7. Subcellular localization of AopW1 in *Nicotiana benthamiana* leaf cells.
Confocal images of *N. benthamiana* leaves 24 h after agroinfiltration. YFP-fused AopW1 from strains M6 (group I) and 7a1 (group II) are shown in yellow. DAPI-stained nuclei are shown in blue. Chloroplasts are shown in red.
(a) Group I AopW1. (b) Group II AopW1. (c) A short variant of group II AopW1 lacking the predicted chloroplast transit peptide (cTP) in its N-terminus ($AopW1_{\Delta 1-85}$). Removal of this region abolishes localization of AopW1 into chloroplasts. White arrows indicate the colocalization of AopW1 with chloroplasts. Scale bars, 20 μm.

et al., 2013). To assess whether AopW1 interacts with the ER, we carried out co-expression assays of AopW1-YFP with the ER marker mRFP-HDEL (Schoberer et al., 2009). All tested AopW1 variants co-localized with the ER (Figure 8b; Figures S6 and S7). While a typical ER organization could be observed following the expression of group II AopW1, group I AopW1 altered the typical ER structure (Figure 8b). In contrast, we were not able to detect clear differences in terms of effects on ER structure between group I (1+2+3) AopW1 and group II (1+2+3+4) AopW1 under tested conditions (Figures S6 and S7).

AopW1 co-localizes with plant endosomes

The plant actin cytoskeleton plays an important role in endocytosis and endosomal trafficking (Paez-Garcia et al., 2018; Thomas et al., 2009). We tested co-localization of AopW1-YFP with various plant endosome markers fused with several fluorescent proteins in *N. benthamiana* leaf cells. The tested markers were DsRed-FYVE, which binds phosphatidyl inositol (Voigt, Timmers, Šamaj, Hlavacka, et al., 2005); AtEHD1-CFP, which partially co-localizes with FYVE, RabD2b (Wave33) and RabA1e (Wave34), and functions in endocytic recycling (Bar, Aharon, et al., 2008; Bar, Benjamin, et al., 2008; Bar et al., 2013); mCherry-Wave33, which possesses endosomal and trans-Golgi localization (Bar et al., 2013); and Ara7 (RabF2b)-CFP, which likely localizes to recycling and late endosomes (Bar et al., 2013; Lee et al., 2004).

Overall, group I and II wild-type versions of AopW1, as well as the analyzed variants- group I (1+2+3) and group II (1+2+3+4)- co-localized with most tested plant endosome markers (Figure 9; Figures S6 and S7), suggesting AopW1

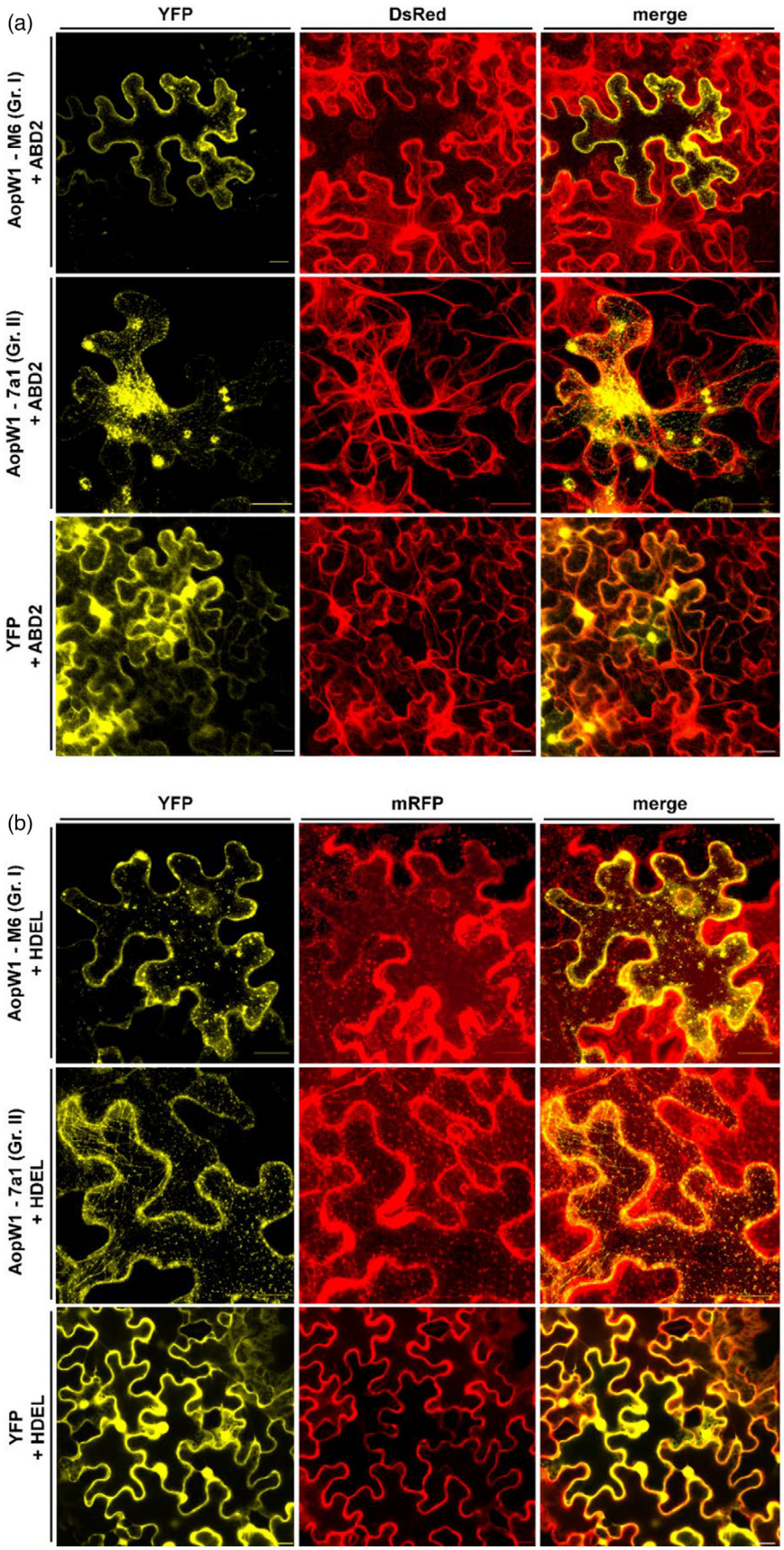

Figure 8. Group I AopW1 disrupts the aactin cytoskeleton and alter the endoplasmic reticulum (ER) distribution in *Nicotiana benthamiana* leaf cells.
Confocal images of *N. benthamiana* leaves 48 and 24 h after agroinfiltration with plant markers and AopW1, respectively. YFP-fused AopW1 from strains M6 (group I) and 7a1 (group II) or YFP alone are shown in yellow. The aactin marker DsRed-ABD2 (a) and the ER marker mRFP-HDEL (b) are shown in red. Scale bars, 20 μm.

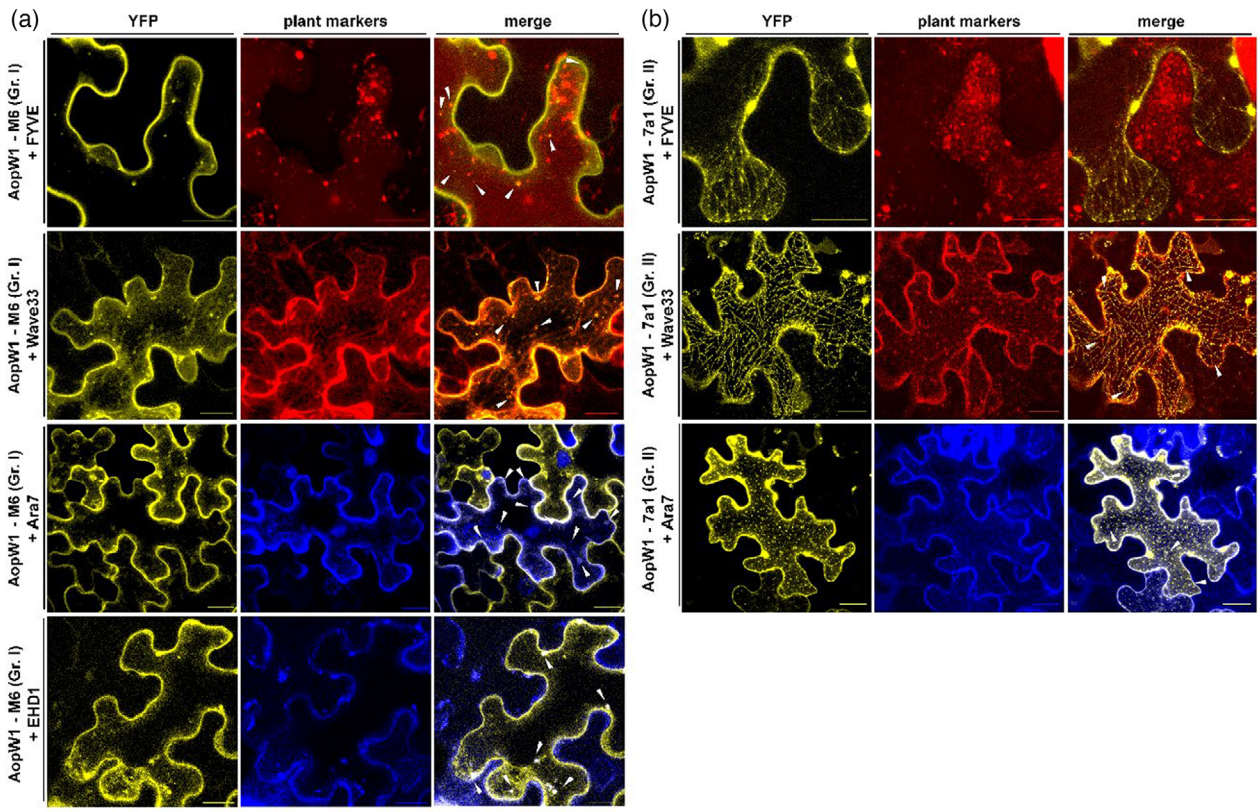

Figure 9. AopW1 co-localizes with plant endosomes in *Nicotiana benthamiana* leaf cells. Confocal images of *N. benthamiana* leaves 48 and 24 h after agroinfiltration with plant markers and AopW1, respectively.
YFP-fused AopW1 from strains M6 [group I (a)] and 7a1 [group II (b)] are shown in yellow. Endosome markers DsRed-FYVE and mCherry-Wave33 (RabD2b) are shown in red. Endosome markers Ara7-CFP (RabF2b) and AtEHD1-CFP are shown in blue. White arrows indicate the co-localization of AopW1 with plant endosomes. The lack of images for the AopW1-7a1/EHD1 combination is due to the fact that we were not able to detect simultaneous signals for these proteins in the same cell. Scale bars, 20 μm.

interferes with early and recycling endosomes. With that said, we were not able to detect co-localization of the group II wild-type version of AopW1 and the endosome marker AtEHD1-CFP. Surprisingly, in contrast to all other tested combinations of AopW1 variants and cell markers, despite many attempts, we could never detect simultaneous signals for group II AopW1 and AtEHD1 in the same cell samples.

EHD1 attenuates AopW1-induced cell death and increases immune responses

Visual observation of *N. benthamiana* leaves used in co-localization experiments indicated that co-infiltration of group I AopW1 with AtEHD1-CFP attenuated the toxic effect induced by the effector. To verify these findings, we carried out additional leaf infiltration assays in which *A. tumefaciens* carrying group I or II AopW1 were infiltrated in combination with *A. tumefaciens* carrying AtEHD1 of free-GFP (control). In agreement with the preliminary observations, results from these experiments confirmed that the expression of EHD1 in *N. benthamiana* substantially attenuates the toxic effects induced by both versions of AopW1 (Figure 6A,B). The visible effects positively correlated with significant reductions in cell death (Figure 6D) and ion leakage (Figure 6F) in the co-expression treatments relative to the expression of the effectors alone.

Similar results were obtained in *A. tumefaciens*-mediated transient expression assays in *N. tabacum* leaves. As similar as in *N. benthamiana*, expression of group I AopW1 in *N. tabacum* leaves induced significantly stronger cell death than group II AopW1; and in both

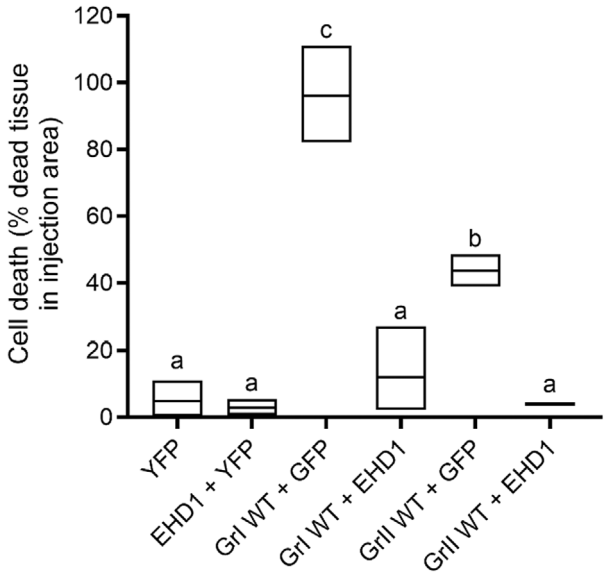

Figure 10. EHD1 attenuates AopW1-induced cell death in *Nicotiana tabacum* leaves.
AopW1 from *Acidovorax citrulli* M6 (group I; Grl WT) and 7a1 (group II; Grll WT) were transiently expressed in *N. tabacum* leaves, with EHD1 (co-infiltration with pBIN19-*Pro35S*:AtEHD1-GFP; Table S2) or without EHD1 (co-infiltration with the control plasmid, pBIN19-*Pro35S*:free-GFP; Table S2). Controls without agroinfiltration of AopW1 variants included infiltration with *A. tumefaciens* carrying pEarleyGate 101 expressing free-YFP (YFP; Table S2). Quantification of cell death was done 3 days after agroinfiltration from three infiltrated leaves per treatment, in three separate experiments. Floating bars represent minimum to maximum values, line in bar represents median. Different letters indicate statistically significant differences among samples in one-way ANOVA with Tukey's *post hoc* test ($P < 0.0006$).

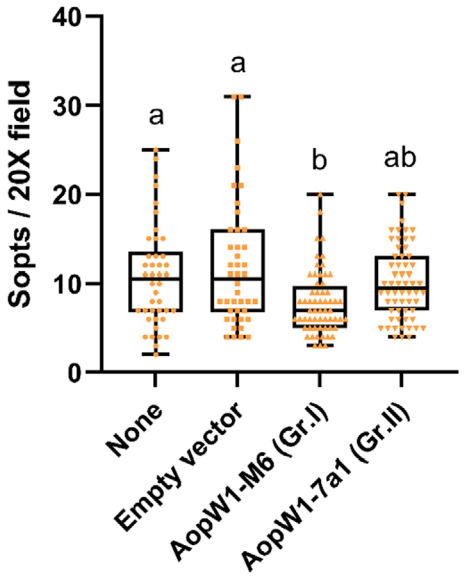

Figure 11. Group I AopW1 reduces callose deposition in *Nicotiana benthamiana* cells after PTI induction.
N. benthamiana leaves were treated with 40 μM flg22 for 24 h and then co-infiltrated with *Agrobacterium tumefaciens* GV3101 carrying pEarleyGate 101, either empty or containing the *aopW1* ORFs of *A. citrulli* M6 (group I) or 7a1 (group II). After 24 h post agroinfiltration, 1-cm diameter disks were collected, stained with aniline blue, and callose deposits were quantified. Callose deposits were counted from six areas from three different leaves from three plants. Data represent means and SE from one experiment out of two with similar results. Letters indicate significant differences among treatments by one-way ANOVA with Tukey's post hoc test ($P < 0.05$).

cases, co-expression with EHD1 significantly attenuated cell death (Figure 10).

EHD1 is known to affect endosomal recycling in Arabidopsis (Bar, Aharon, et al., 2008; Bar et al., 2013). We asked whether EHD1 could be directly involved in plant immunity. For this purpose, we transiently co-expressed EHD1 and the fungal defense elicitor ethylene-inducing xylanase (EIX; Dean et al., 1991; Ron & Avni, 2004) in leaves of *N. tabacum*, and monitored EIX-induced cell death 72 h post-transformation. Leaves co-expressing EIX and EHD1 showed significantly higher levels of induced cell death than leaves expressing EIX alone (Figure S8a). Similarly, *N. tabacum* leaves transiently transformed with EHD1 showed significantly increased levels of ethylene biosynthesis than non-transformed leaves following treatment with EIX (Figure S8b).

Group I AopW1 reduces callose deposition in *N. benthamiana* leaves after PTI induction

Increased callose deposition is a common marker of PTI and many pathogen effectors are able to reduce callose deposition upon induction of PTI (Voigt, 2014; Wang et al., 2021). To assess whether AopW1 affects callose deposition, *N. benthamiana* leaves were treated with the flagellin-derived PTI elicitor flg22 (Felix et al., 1999). After 24 h, leaves were agroinfiltrated with group I or II AopW1. Leaf samples were collected after 24 h for assessment of callose deposition. As controls, leaves were left untreated or infiltrated with *A. tumefaciens* GV3101 carrying pEarleyGate 101 (empty vector). Group I AopW1 significantly reduced the number of callose deposits induced by flg22, as compared with controls. In contrast, group II AopW1 did not significantly differ from controls in terms of callose deposition (Figure 11).

Sequence variation in AopW1 is involved in host adaptation

Melon and watermelon are the most common hosts of *A. citrulli*, with group I strains being better adapted to melon and group II strains to watermelon (Burdman et al., 2005; Walcott et al., 2000, 2004). Traore et al. (2019) showed that group I and II strains impaired in *aopW1* have compromised virulence in melon and watermelon, respectively (Traore et al., 2019). Here we asked how impairment of *aopW1* affects the abilities of *A. citrulli* to establish and cause disease in the less preferred host. We also asked how complementation of the mutant strains with *aopW1* from the other group affects the interactions of both strains with the two hosts. In these experiments, melon

and watermelon leaves were spray-inoculated with mutants and complemented strains that were generated in the background of the group I and II strains, M6 and 7a1, respectively.

Disease severity data, expressed as percentage of lesion area relative to the whole leaves, are summarized in Figure 12, and representative images of inoculated leaves are shown in Figures S9–S12. As expected, M6 and 7a1

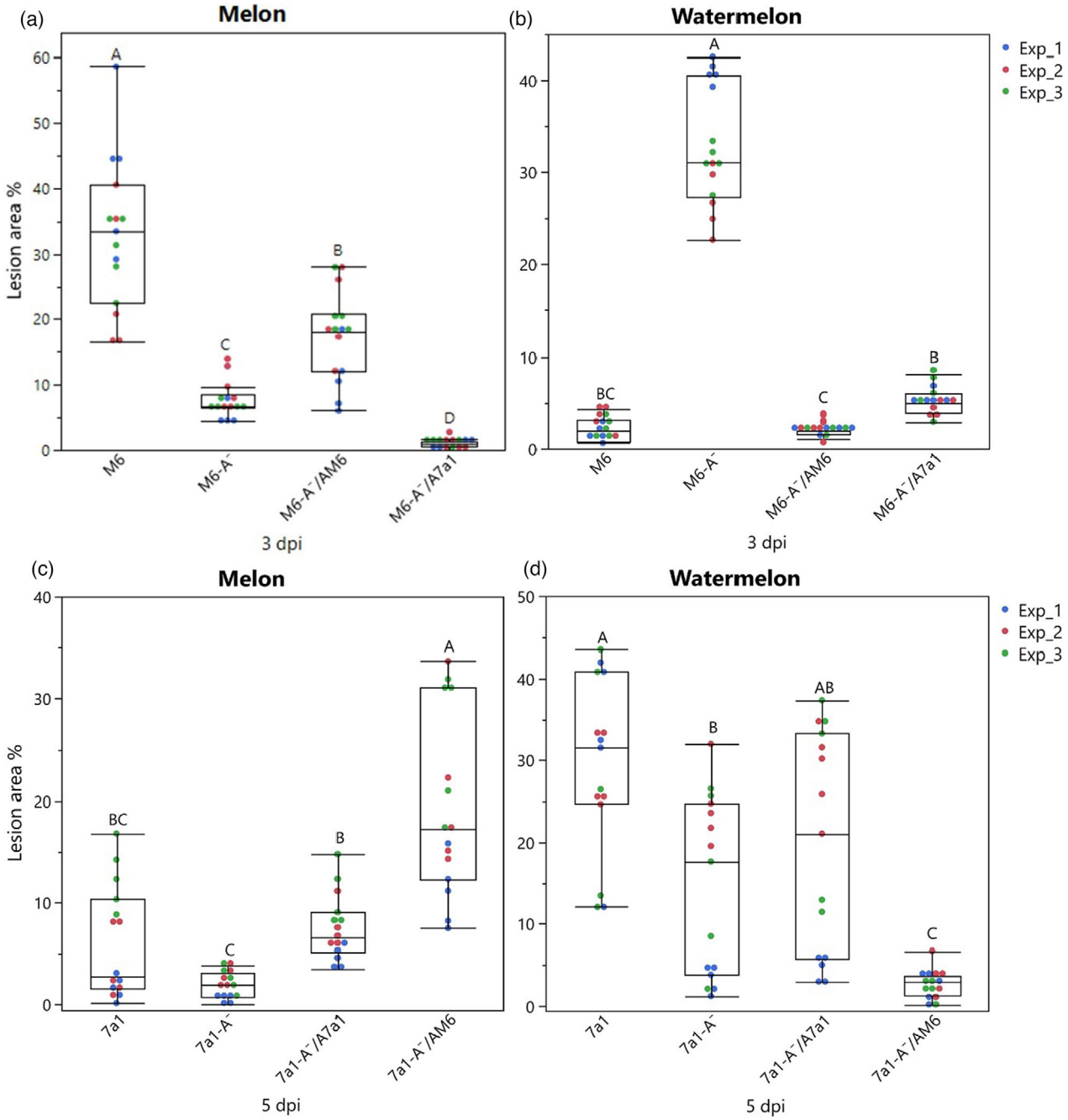

Figure 12. Disease severity of melon and watermelon leaves inoculated with different strains of *Acidovorax citrulli*.
Melon (a, c) and watermelon (b, d) leaves were spray-inoculated with bacterial suspensions as described in "Experimental Procedures" section. Disease severity was assessed by measuring the symptomatic area 3 or 5 days post inoculation (dpi), and calculating the percentage of this area relative to the whole leaf. Strains were wild-type M6 and 7a1; M6-A⁻ and 7a1-A⁻, M6 and 7a1 mutants defective in *aopW1*; M6-A⁻/AM6 and M6-A⁻/A7a1, M6-A⁻ mutant carrying a plasmid with *aopW1* from strains M6 and 7a1, respectively; and 7a1-A⁻/AM6 and 7a1-A⁻/A7a1, 7a1-A⁻ mutant carrying a plasmid with *aopW1* from strains M6 and 7a1, respectively. Boxplots represent minimum to maximum values with inner quartile ranges (box), outer quartile ranges (whiskers), and median (line in box). Data are from three independent experiments (Exp_1 to Exp_3), with five replicates (leaves) per treatment per experiment (data from each experiment are shown with different colors). Different letters indicate statistically significant differences ($P < 0.05$) among samples based on one-way ANOVA with Tukey's post hoc test.

mutants impaired in *aopW1*, were significantly ($P < 0.05$) compromised in their ability to cause disease on their preferred hosts, melon and watermelon, respectively. Also as expected, introduction of a plasmid carrying *aopW1* from the corresponding group to the mutants provided partial complementation in terms of virulence ability on the preferred hosts. Interestingly, introduction of *aopW1* from the other group caused a severe and significant ($P < 0.05$) decrease in virulence in the preferred hosts in both groups I and II strains (Figure 12a,d).

In line with the above results, abolishment of *aopW1* in strain M6 significantly ($P < 0.05$) and dramatically increased the ability of this strain to cause disease in watermelon leaves. Introduction of both versions of *aopW1* to the M6 *aopW1*$^{-}$ mutant significantly ($P < 0.05$) reduced its virulence activity on watermelon, although the mutant strain that carried the group II version was significantly ($P < 0.05$) more virulent than the one carrying the group I version (Figure 12b).

A quite different picture was observed in the interaction between strain 7a1 and its less preferred host, melon. While a slight tendency was observed that showed lower values of percentage of disease area in leaves inoculated with the *aopW1*$^{-}$ mutant as compared with wild-type 7a1, these differences were not statistically significant. Moreover, introduction of both group I and II versions of *aopW1* to the mutant significantly ($P < 0.05$) increased its virulence on melon. In line with the observed importance of *aopW1* in terms of contribution to virulence of the group I strain in melon (Figure 12a), the 7a1 *aopW1*-mutant carrying group I *aopW1* exhibited significantly ($P < 0.05$) higher virulence than wild-type 7a1 and the other 7a1-derived strains in this plant (Figure 12c).

Overall, disease severity data obtained in these experiments strongly correlated with measurements of ion leakage in inoculated leaves (Figure S13), and with bacterial concentrations in infected leaves (Figure 13). These measurements also support a significant contribution *aopW1* to disease induction ability and establishment of *A. citrulli* in the preferred hosts. On the other hand, they also strengthen the notion that the group II version of *aopW1* restricts the establishment and virulence of *A. citrulli* in melon (Figure 13a,c; Figure S13a,c), whereas the group I version of this effector restricts these pathogen abilities in watermelon (Figure 13b,d; Figure S13b,d).

DISCUSSION

Acidovorax citrulli requires a functional T3SS to cause disease (Bahar & Burdman, 2010; Johnson et al., 2011). A large number of novel T3E genes have been recently identified in the genome of the *A. citrulli* model strain M6 (Jiménez-Guerrero et al., 2020). M6 belongs to one of the two predominant groups of *A. citrulli* strains, group I, which is composed of strains that were mainly isolated from melon plants. The second major group of strains, group II, is composed of strains that show preferential association with watermelon and can be clearly distinguished by genetic and biochemical traits from group I strains (Burdman et al., 2005; Eckshtain-Levi et al., 2016; Feng et al., 2009; Walcott et al., 2000, 2004). We have shown that group I and II strains differ in their T3E arsenal. Firstly, several T3Es appear to be group-specific. Secondly, many T3E genes that are shared by the two groups show significant differences in their sequences (Eckshtain-Levi et al., 2014; Jiménez-Guerrero et al., 2020). In this study, we characterized an *A. citrulli* T3E, AopW1, which belongs to the second category.

AopW1 shares similarity with *P. syringae* HopW1, and with T3Es from other plant-pathogenic bacterial species, including *Acidovorax* spp. (Jiménez-Guerrero et al., 2020; Figure 3). This effector was recently shown to contribute to *A. citrulli* virulence (Traore et al., 2019). In the present study, heterologous expression in yeast revealed that while group I AopW1 is extremely toxic to these cells, the group II version of this effector has only a minor toxic effect (Figure 1). Remarkably, similar differences in cytotoxic ability between group I and II AopW1 were further detected in *N. benthamiana* (Figure 6) and *N. tabacum* (Figure 10).

Among AopW1 homologous effectors, the only one that was well characterized is *P. syringae* HopW1. While *aopW1* encodes a product of 485 a.a., HopW1 is 774 a.a-long. In fact, AopW1 shares similarities with the central and C-terminal parts of HopW1. Lee et al. (2008) showed that HopW1 triggers immunity responses in the Arabidopsis Ws ecotype and in *N. benthamiana*. The authors also showed that HopW1 interacts with a putative acetylornithine transaminase (WIN1), a protein phosphatase (WIN2), and a firefly luciferase superfamily protein (WIN3) of Arabidopsis, with the HopW1 C-terminal domain being required for these interactions. Later, Kang et al. (2014) showed that HopW1 promotes virulence in a different Arabidopsis ecotype, Col-0, by inhibiting actin polymerization and severely disrupting endosome trafficking.

AopW1 is highly conserved among group I and II strains of *A. citrulli*, except for a HVR located at a.a. positions 147–192, and showing 14 a.a. differences between group I and II strains (Figure 3b). Importantly, the HVR is included in the part of AopW1 that shares similarities with the central and C-terminal regions of HopW1 that are required for cytotoxic activity. Here we showed that deletion of the HVR abolishes the ability of group I AopW1 to exert toxic effects on yeast (Figure 5). We also noticed that among the 14 variable a.a. positions between group I and II AopW1 in the HVR, six are well conserved between group I AopW1, HopW1, and other HopW1 homologs, but not group II AopW1 (Figure 3b). We therefore hypothesized that these positions are critical for the cytotoxic activity of

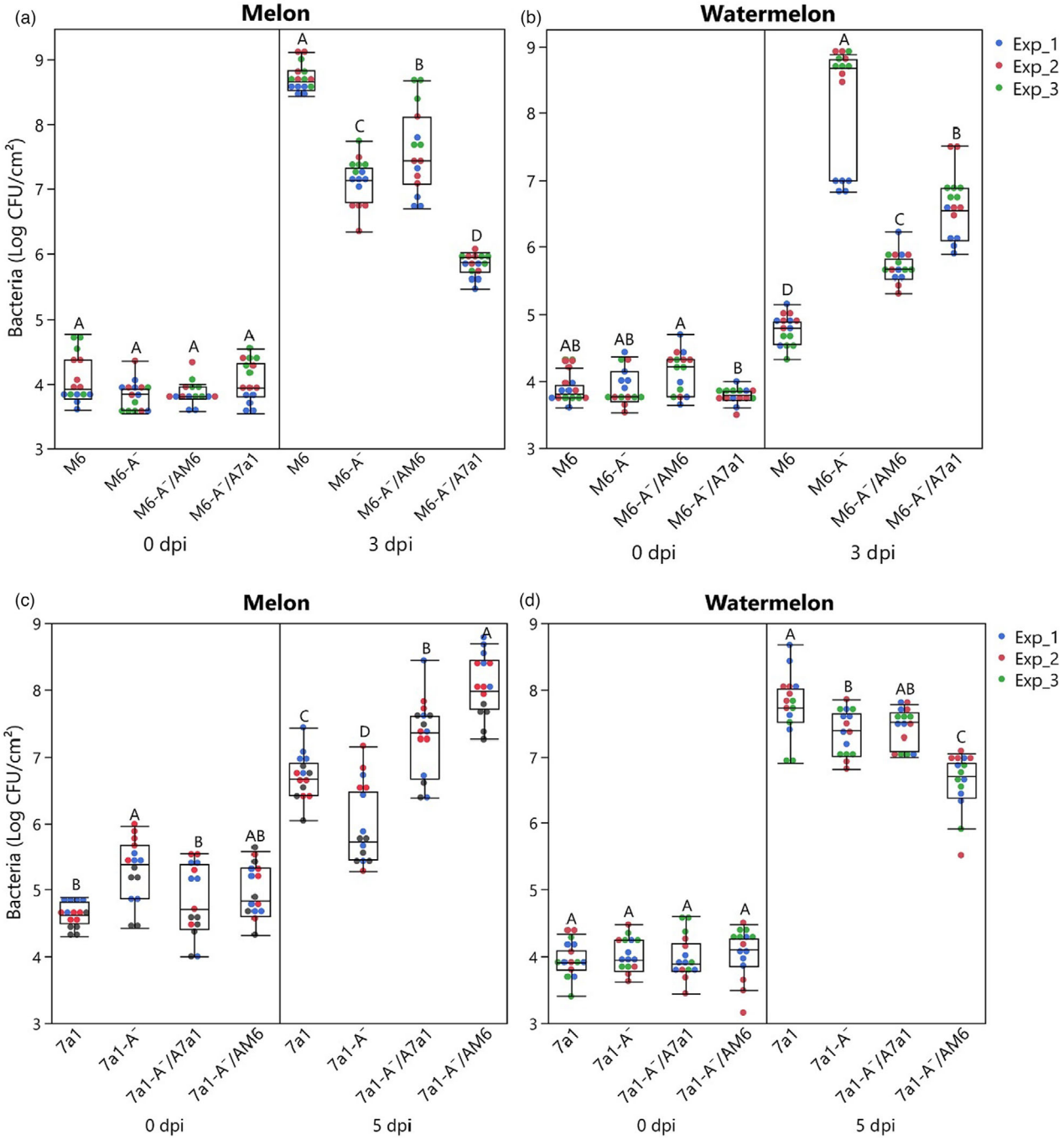

Figure 13. Establishment of *Acidovorax citrulli* strains in leaves of melon and watermelon.
Melon (a, c) and watermelon (b, d) were spray-inoculated with the *A. citrulli* strains described in Figure 12. Bacterial concentrations in inoculated leaves were determined following colony counting of serially-diluted leaf extracts as described in Experimental Procedures, at 0 and 3 or 5 dpi. Boxplots represent minimum to maximum values with inner quartile ranges (box), outer quartile ranges (whiskers), and median (line in box). Data are from three independent experiments (Exp_1 to Exp_3), with five replicates (leaves) per treatment per experiment (data from each experiment are shown with different colors). Different letters indicate statistically significant differences ($P < 0.05$) among samples based on one-way ANOVA with Tukey's post hoc test.

AopW1, HopW1, and other effectors of this family. In support of this notion, growth inhibition assays of yeast expressing AopW1 variants in which selected positions were swapped to the a.a. present in the other group, revealed that a combination of three substitutions in the HVR [V-154-I, R-162-Q, and P-167-A; group I (1+2+3 AopW1)] was sufficient to cause a significant reduction of cytotoxicity exerted by group I AopW1. On the other hand,

a combination of four substitutions [I-154-V, Q-162-R, A-167-P, and T-174-A; group II (1+2+3+4) AopW1] conferred high cytotoxic ability to the group II version of AopW1 (Figure 4). The effects of these substitutions were further validated *in planta*: while the group I (1+2+3) AopW1 variant was less toxic to *N. benthamiana* cells than group I AopW1, the group II (1+2+3+4) AopW1 variant was significantly more toxic than its parental effector (Figure 6). Overall, these results demonstrate the important role of the above a.a. positions for the cytotoxic activity of AopW1 and probably of other effectors that belong to the HopW1 family.

The actin cytoskeleton is a complex network of dynamic polymers that play important roles in a wide range of cellular processes (Mishra et al., 2014; Pollard & Borisy, 2003). It also plays an essential role in plant immunity, assisting in multiple defense functions in both early and late defense responses, such as vesicle trafficking and endo/exocytosis, fortification of the cell wall, and deposition of callose (Hardham et al., 2007; Li & Staiger, 2018; Voigt, 2014). Upon bacterial infection, epidermal cells of Arabidopsis leaves show early increase in density of actin filaments and late actin remodeling, with these responses being correlated with PTI and effector-triggered susceptibility, respectively (Henty-Ridilla et al., 2013). Therefore, it is not surprising that pathogen effectors target host cytoskeletal organization in order to subvert plant defense responses, as demonstrated for HopW1 (Kang et al., 2014) but also for a different *P. syringae* effector, HopG1 (Shimono et al., 2016). In addition, several studies indicate that other *P. syringae* effectors, HopAV1, HopAZ1, HopZ1a, and HopE1, as well as AvrBsT from *Xanthomonas euvesicatoria*, and the powdery mildew effector ROPIP1, could be acting to some extent on the plant cell cytoskeleton (Cheong et al., 2014; Choi et al., 2017; Guo et al., 2016; Lee et al., 2012; Nottensteiner et al., 2018).

In this study, we showed that group I AopW1 disrupts muscle F-actin *in vitro* (Figure 2), and affects yeast and plant filamentous actin (F-actin) *in vivo* (Figure 8a; Figure S2). Findings from our study also support that group II AopW1 is an attenuated version of this effector in terms of actin disruption ability (Figure 8a; Figure S2). We also showed that group I but group II AopW1 is able to significantly reduce callose deposition in *N. benthamiana* leaves pre-treated with the PTI elicitor flg22 (Figure 11). This could be explained, at least partially, by the severe disruption of the actin cytoskeleton by group I but not by group II AopW1. Differences between the two versions of the effector were also observed in the alteration of the ER structure (Figure 8b), which could be a result of the differences between the effectors in actin disruption ability.

Actin is directly involved in vesicle trafficking and endo/exocytosis processes that are essential for the delivery of specialized proteins and defense molecules to the cytoplasmic membrane (Li & Staiger, 2018). Several defense receptors are internalized into early endosomes, and further recycled back to the membrane via recycling endosomes, or targeted for degradation via the late endosome pathway. Increase in the amount of a receptor in endosomes causes a concomitant signaling enhancement, whereas abolishment of endosome formation once the receptor is internalized causes signaling attenuation (Bar & Avni, 2014). Therefore, endosome components appear to be attractive targets of pathogen effectors. As mentioned above, HopW1 was shown to reduce the number of endosome vesicles *in planta* (Kang et al., 2014). Other T3Es seem to be associated with plant endosomes, such as HopM1 from *P. syringae*, which interferes with AtMIN7/BEN1 function at the early endosome/trans-Golgi network (TGN) (Nomura et al., 2006, 2011). In our study, both group I and group II AopW1, as well as their mutated variants co-localized with endosome markers, supporting that it acts in some way in early and recycling endosome functioning (Figures 9 and 14; Figures S6 and S7).

Co-localization of EHD1 with FYVE and Wave33 was reported by Bar, Aharon, et al. (2008) and Bar et al. (2013), who suggested a role for this protein in endocytic recycling. The mammalian EHD1 homologs are known to be involved in endocytic recycling (Galperin et al., 2002; Grant & Caplan, 2008). Moreover, it has been shown that overexpression of EHD1 protects against salinity stress, suggesting an association between endocytic recycling and plant stress coping mechanisms (Bar et al., 2013). Here we showed that overexpression of EHD1 significantly attenuates the cytotoxic effects induced by group I and group II AopW1 in *N. benthamiana* (Figure 6) and *N. tabacum* (Figure 10) leaves, thus supporting the involvement of this effector in endocytic recycling. Interestingly, in all experiments involving co-infiltration of AopW1 and EHD1, we were not able to detect simultaneous signals for group II AopW1 and EHD1 in the same cell (Figure 9). While this result suggests a strong attenuation of group II AopW1 toxicity by EHD1, we cannot exclude the possibility that group II AopW1 may destroy structures labeled by EHD1. In addition, while we cannot exclude the possibility that EHD1 may decrease expression or stability of AopW1, we showed that transient expression of EHD1 in *N. tabacum* leaves increases defense responses induced by the EIX elicitor (Figure S8), thus supporting that increased endocytic recycling mediated by EHD1 could contribute to plant immunity.

Chloroplasts play an important role in plant immunity as they are the source of important defense signaling molecules (Nomura et al., 2012; Serrano et al., 2016; Singh et al., 2018). AopW1 possesses a predicted cTP signal in its N-terminal part (Appendix S1) and co-localization of AopW1 to chloroplasts in a cTP signal-dependent manner was demonstrated in this study (Figure 7). Whether AopW1

interferes with chloroplast functioning or with a chloroplast signaling pathway is yet to be determined.

In this study, we found that group I AopW1 is much more toxic than group II AopW1 to yeast, *N. benthamiana* and *N. tabacum* cells. On the other hand, Traore et al. (2019) showed that AopW1 contributes to virulence of both group I and II strains of *A. citrulli*. This apparent discrepancy could be explained by the fact that *A. citrulli* is much more adapted to cucurbits than to yeast or tobacco; thus, it is not surprising that group II AopW1 has a more significant effect in watermelon than in heterologous organisms. Yet, in this study, we found that the abolishment of *aopW1* in the group I strain had a more dramatic effect on virulence and colonization abilities on melon leaves, than the effect observed for abolishment of *aopW1* in the group II strain-watermelon interaction (Figures 12 and 13). Remarkably, group I AopW1 was shown to restrict virulence and colonization of *A. citrulli* in watermelon leaves, whereas group II AopW1 caused a similar effect on melon leaves. Overall, inoculation experiments with melon and watermelon carried out in this study support that AopW1 has a critical role in shaping pathoadaptation of *A. citrulli* to its major host plants, likely by inducing toxicity in the matched host while eliciting immune responses in the less suitable host. Interestingly, as mentioned above, the *P. syringae aopW1*-homolog *hopW1* was shown to promote virulence in *A. thaliana* Col-0 (Kang et al., 2014), while triggering a strong immune response in a different ecotype of this species, Ws (Lee et al., 2008).

In conclusion, our study provides insights into mechanistic features of T3Es belonging to the HopW1 family. While it was previously shown that group I and II strains of *A. citrulli* possess different versions of AopW1 (Eckshtain-Levi et al., 2014), here we show that these versions substantially differ in their ability to interact with plant cell compartments and disrupt the actin cytoskeleton (Figure 14). We also show that genetic variation in AopW1 is an important determinant of differences in preferential association between the two groups of *A. citrulli* strains. In other words, variation in AopW1 seems to be among the significant evolutionary alterations that occurred during the process of adaptation of *A. citrulli* to different hosts. In view of the relatively large amount of T3E genes in *A. citrulli*, and the genetic variation of T3E genes among group I and II strains, it is reasonable to assume that additional T3Es contribute to the differences in host preference between the groups. It is worth remarking that a similar variation in the AopW1 HVR occurs among strains of *Acidovorax avenae*, which are pathogenic to several graminaceous plants. It would be interesting to investigate whether AopW1 homologs in *A. avenae* play a similar role in adaptation to different graminaceous species.

EXPERIMENTAL PROCEDURES

Strains, plant material, and growth conditions

Strains and plasmids used in this study are listed in Table S2. *Escherichia coli* and *A. tumefaciens* as well as derived strains were cultured in Luria-Bertani (LB; Difco Laboratories, Franklin Lakes, NJ, USA) medium at 37°C and 28°C, respectively. *A. citrulli* strains were grown in nutrient broth (NB; Difco Laboratories) or nutrient agar (NA; NB containing 15 g L^{-1} agar) at 28°C. When required, the media were supplemented with the antibiotics ampicillin (Ap, 100 μg ml^{-1} for *E. coli*, and 200 μg ml^{-1} for *A. citrulli*), rifampicin (Rif, 50 μg ml^{-1}), kanamycin (Km, 30 μg ml^{-1} for *E. coli* and 50 μg ml^{-1} for *A. tumefaciens*), and gentamycin (Gm, 10 μg ml^{-1}). *Saccharomyces cerevisiae* BY4741 (Brachmann et al., 1998) was grown at 30°C on YPD medium (Rédei, 2008). For repressing and inducing conditions, BY4741-derived strains were grown in selective synthetic complete medium without leucine supplemented with 2% glucose or 2% galactose and 1% raffinose, respectively (Salomon & Sessa, 2010). *N. benthamiana* plants (Goodin et al., 2008) were grown in a growth chamber under the following controlled conditions: 16 h at 26°C in the light and 8 h at 18°C in the dark, 70% humidity. *N. tabacum* cv. Samsun NN plants were grown in a greenhouse under long-day conditions (16 h light/8 h dark), at 25°C. Melon (*Cucumis melo*) cv. Rachel and watermelon (*Citrullus lanatus*) cv. Lahat (both from Hazera Genetics, Berurim, Israel) were grown in a greenhouse at 16 h light/8 h dark at 27°C.

Molecular manipulations

Routine molecular manipulations and cloning procedures were carried out by standard techniques unless stated otherwise. Restriction enzymes and T4 DNA ligase were purchased from Fermentas (Thermo Fisher Scientific, Waltham, MA, USA). AccuPrep® Plasmid Mini Extraction Kit (Bioneer Corporation, Daejeon, Republic of Korea) and Wizard® SV Gel and PCR Clean-Up System (Promega Corporation, Madison, WI, USA) were used for plasmid and PCR product extraction and purification, respectively. Bacterial DNA was extracted using the GeneElute Bacterial Genomic DNA Kit (Sigma-Aldrich, St. Louis, MO, USA). All constructs were verified by DNA sequencing at Hy Laboratories (Rehovot, Israel). PCR primers were purchased from Hy Laboratories or Sigma-Aldrich Israel (Rehovot, Israel). All oligonucleotide primers used in this study are listed in Table S4. PCR reactions were performed with the Readymix Red Taq PCR reactive mix (Sigma-Aldrich), Phusion high-fidelity DNA polymerase (Fermentas, Burlington, Canada), or with the Q5® High-Fidelity DNA Polymerase (New England Biolabs, Ipswich, MA, USA) using an Eppendorf (Hamburg, Germany) thermal cycler.

Gel electrophoresis and Western blotting

For immunostaining, proteins were separated by SDS-PAGE and electroblotted using the iBlot Gel Transfer Stacks (Invitrogen, Carlsbad, CA, USA) and iBlot Transfer Device (Invitrogen), following the manufacturer's instructions. Nitrocellulose membranes were blocked with TBS containing 0.1% (v/v) Tween 20 and 3% (w/v) skim milk and incubated with antibodies raised against c-Myc, His and HA (Cell Signaling Technology, Danvers, MA, USA) diluted 1:1000 in the same solution. Anti-mouse or anti-rabbit HRP-linked antibodies (Cell Signaling Technology) were used as secondary antibodies. Reactions were visualized using a chemiluminescent substrate (Cyanagen, Bologna, Italy) in a LAS500 apparatus (GE Healthcare, Chicago, IL, USA).

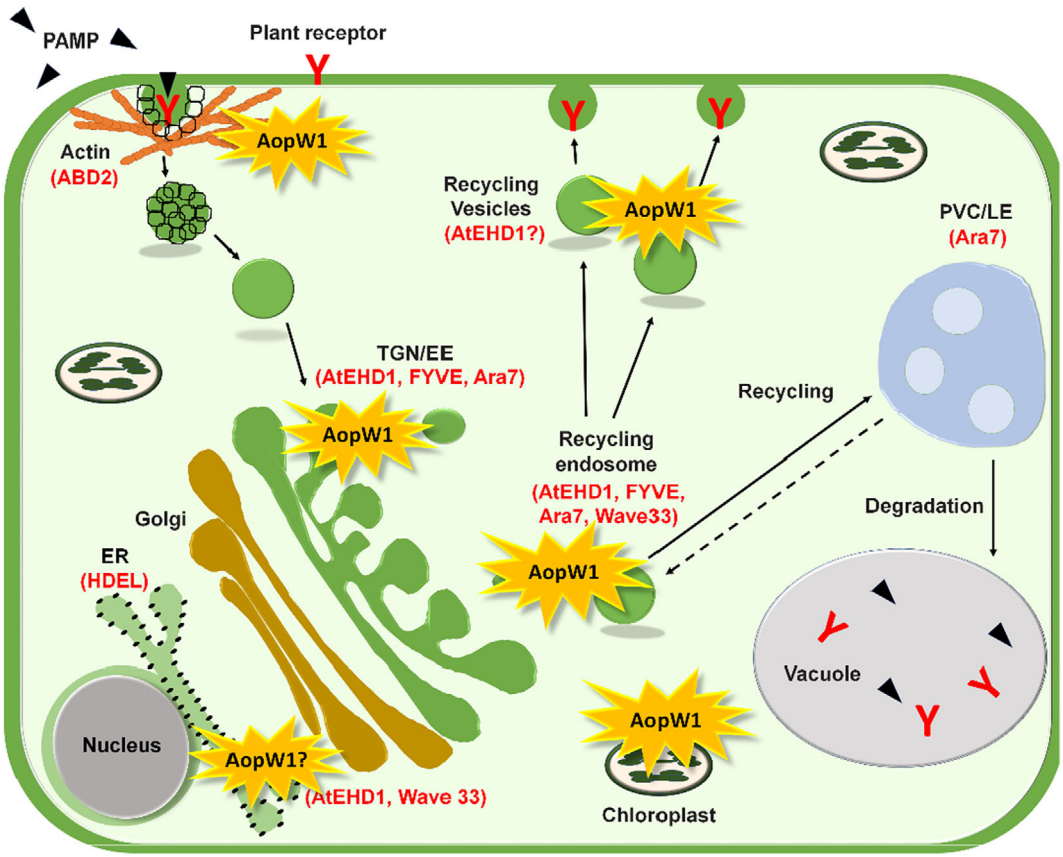

Figure 14. Schematic representation of AopW1 localization and targeting in the plant cell.
AopW1 localizes at the cell cytoplasm, where it disrupts aactin filaments and co-localizes with early and recycling endosomes. AopW1 also localizes with chloroplasts. Co-localization with known markers is indicated in red (AtEHD1, FYVE, Ara7, HDEL, and Wave33). Arrows point to trafficking pathways from the membrane to the early/re-cycling endosome and back to the membrane. TGN/EE, trans-Golgi network/early endosome; MVBs/LE, multivesicular bodies/late endosome.

Cloning and transformation of yeast

For expression in yeast, the *aopW1* ORFs of *A. citrulli* M6 and 7a1 were PCR-amplified with specific primers. The obtained products were inserted into the *Bam*HI/*Eco*RI sites of pGML10 (Iha & Tsurugi, 1998), following pretreatment of the inserts and plasmids with the same restriction enzymes. The ORFs of the *hopW1* gene of *P. syringae* pv. *maculicola* ES4326 and of the *hopW1* homologous gene of *X. translucens* pv. *translucens* (*Xtt*) DSM 18974 were cloned into pGML10 by the restriction-free method (van den Ent & Lowe, 2006) using appropriate primers, and plasmid pBAV154-dexHopW1-HA or genomic DNA of *Xtt* DSM 18974 as templates, respectively. The mutated variants of AopW1 were generated by inserting mutations in the corresponding primers in combination with the Quick Change Lightening Site-Directed Mutagenesis kit (Agilent Technologies, Santa Clara, CA, USA). For this purpose, PCR reactions for each mutation were carried out in 50 μL reaction mixture containing 5 μl of 10× reaction buffer, 100 ng of template DNA, 125 ng of both oligonucleotide primers, 1 μl of dNTP mix, 1.5 μl of Quick Change solution reagent and 1 μl of Quick Change lightening enzyme. The final volume was made with sterilized distilled water (SDW). The cycling parameters included an initial denaturation step at 95°C for 2 min, 18 cycles of denaturation (at 95°C for 20 sec), annealing (at 60°C for 10 sec), and extension (at 68°C for 2.5 min), and final extension at 68°C for 5 min. Then, the amplified plasmid DNA product was digested with *Dpn*I provided with the kit. Effector gene variants carrying combinations of individual mutations in the background of the M6 and 7a1 *aopW1* genes were generated using the same procedure. The resulting plasmids were mobilized into *S. cerevisiae* BY4741 by the lithium acetate yeast transformation method (Gietz et al., 1992). Transformed yeast cells were plated onto selective synthetic complete without leucine medium supplemented with 2% glucose.

Yeast growth inhibition and viability assay

Growth inhibition assays were performed as described (Salomon et al., 2011). *S. cerevisiae* BY4741 carrying pGML10 with *aopW1* ORFs were grown at 30°C overnight in liquid selective medium containing 2% glucose. Cultures were centrifuged (800 ***g***, 5 min, at room temperature; twice) and pellets were suspended with SDW to an optical density at 600 nm (OD_{600}) of 1.0. For each culture, four serial dilutions were prepared and 10-μl aliquots from each dilution were spotted onto solid selective medium containing 2% glucose (repressing medium), or 2% galactose and 1% raffinose (inducing medium), or onto inducing medium supplemented with 7 mM caffeine, 1 M sorbitol or 0.5 M sodium chloride. Yeast cells were incubated at 30°C for 3 days.

For yeast viability assays, overnight cultures of yeast (as detailed above for growth inhibition assays) were diluted with

fresh repressing medium to an OD_{600} of 0.5, and incubated for 2 h at 30°C with shaking (200 rpm). Yeast cells were washed as described above but pellets were resuspended in 2 ml of induction medium to an OD_{600} of 0.2. The resulting cultures were incubated at 30°C with shaking (200 rpm) and 0.1-ml aliquots were collected at different time points. The concentrations of viable cells were determined by plating of serial dilutions on selective repressing medium, with plates being incubated for 2 days at 30°C. The expression of the effectors was validated by Western blot analysis, following the procedure described by Salomon and Sessa (2010), using a c-Myc primary antibody.

Yeast actin staining

Yeast actin staining was performed as described (Adams & Pringle, 1991), with some modifications. Yeast overnight cultures grown as described above were diluted with fresh repressing medium to an OD_{600} of 0.4 and incubated for 2 h at 30°C with shaking (200 rpm). Yeast cells were washed as described above and pellets were resuspended in 4 ml inducing medium to an OD_{600} of 0.2. Cultures were incubated at the same conditions for 8 h to allow effector expression. During this period, cultures were refreshed with inducing medium at least once. Cultures were then centrifuged (800 ***g***, 5 min, at room temperature), and pellets were washed with phosphate-buffered saline solution (PBS; 137 mM NaCl, 2.7 mM KCl, 8 mM Na_2HPO_4 and 2 mM KH_2PO_4; pH 7.2). Pellets were carefully resuspended in 1 ml of fresh paraformaldehyde 4% solution in PBS. Fixation was done by incubation at 4°C for 15 min with soft rotation. Cells were washed by centrifugation (500 ***g***, 5 min, at room temperature) and resuspension with PBS twice, and finally resuspended in 1 ml of fresh PBS with 0.1% Triton X-100. The suspensions were incubated at room temperature for 20 min, after which the cells were washed as described above with PBS (twice). For staining of yeast cell actin and nucleus, the pellets were resuspended with 100 μl of blocking solution (1× PBS, 1% BSA and 0.1% saponin) containing 50 μg ml^{-1} of TRITC-phalloidin (Sigma-Aldrich) and 2.5 μg ml^{-1} of 4′,6-diamidino-2-phenylindole (DAPI; Sigma-Aldrich) (Kapuscinski & Skoczylas, 1977). The suspensions were incubated for 1 h at 4°C, at dark conditions. Cells were then washed twice by centrifugation and resuspension with PBS as described above and finally resuspended in 5–10 μl of 0.1 M propyl gallate in 100% glycerol. One-microliter drops of the suspensions were visualized in a Leica SPE Confocal Microscope (Leica Microsystems, Wetzlar, Germany), using poly-L-lysine microscope slides.

Expression and purification of recombinant AopW1 for F-aactin disruption assays

The *aopW1* ORFs without their 300-bp N-terminal region were amplified by PCR with specific primers. The resulting fragments were cloned into the *Eco*RI/*Xho*I site of pET28a, leading to generation of recombinant AopW1 fused to polyhistidine tag (His-tag) in both extremes. The generated plasmids were mobilized into *E. coli* BL21(DE3) (Studier & Moffatt, 1986) by the heat shock method (Froger & Hall, 2007).

Expression and purification of recombinant His-tagged AopW1 was performed following the protocol described by the Macherey-Nagel (Duren, Germany) Purification of His-tag Protein manual. For expression of AopW1, *E. coli* BL21(DE3) carrying plasmids pET28a::$_{M6}$*aopW1-M6*$_{\Delta 1-100}$ or pET28a::$_{7a1}$*aopW1-7a1*$_{\Delta 1-100}$ (encoding His-tagged $AopW1_{101-485}$ from strains M6 and 7a1, respectively) were grown in 5 ml of LB supplemented with kanamycin at 37°C overnight. Cultures were then transferred to 100 ml of the same medium and incubated at 37°C until the OD_{600} reached to 0.6. Expression was induced by addition of 1 mM isopropyl β-D-1-thiogalactopyranoside (IPTG). After 4 h, cells were resuspended in NPI buffer (50 mM NaH_2PO_4, 300 mM NaCl; pH 8.0), containing 10 mM imidazole (BioWorld, Dublin, OH, USA), harvested by centrifugation at 6000 ***g*** for 15 min at 4°C, and stored at −80°C until use.

For purification of recombinant proteins, pellets from 100 ml of IPTG-induced cultures were resuspended in 3 ml of NPI buffer containing 1 mM imidazole, 1 mM phenylmethanesulfonyl fluoride, 1× protease inhibitor cocktail (Bimake, USA) and 1 mg ml^{-1} lysozyme. Suspensions were incubated on ice for 30 min, and then sonicated on ice 10 times for 15 sec, with 15-sec cooling intervals between sonication treatments. The lysate was clarified by centrifugation at 10 000 ***g*** (30 min, at 4°C). Half of the clarified lysate was incubated at 4°C for 90 min in a column containing 130 μl of Protino Ni-NTA agarose (Macherey-Nagel), previously equilibrated with NPI buffer (pH 8.0), containing 10 mM imidazole, allowing binding of His-tagged AopW1 to Protino Ni-NTA agarose. Columns were washed twice with 500 μl of NPI buffer containing 100 mM imidazole, and once with 500 μl of NPI buffer containing 200 mM imidazole. His-tagged AopW1 was eluted by adding twice 50 μl of NPI buffer containing 500 mM imidazole. Purified proteins were dialyzed using 10 000 MWCO Slide-A-Lyzer Dialysis Cassettes (Thermo Fisher Scientific) and concentrated using Amicon Ultra-4 Centrifugal Filter Unit (Millipore Sigma, Burlington, MA, USA), following the manufacturer's instructions. Expression and purification of His-tagged AopW1 were verified by SDS-PAGE and confirmed by Western blot using His-tag monoclonal antibodies.

Non-muscle F-actin disruption assays

F-actin disruption assays were carried out in the presence of purified recombinant $AopW1_{101-485}$, according to Kang et al. (2014) with few modifications, using the Actin Binding Protein Spin-Down Assay Biochem kit (Cytoskeleton, Denver, CO, USA). Briefly, non-muscle actin was polymerized to actin filaments (F-actin) in 10 mM Tris, 1 mM ATP, 50 mM KCl, 1 mM EGTA, 0.2 mM $CaCl_2$, and 2 mM $MgCl_2$ (pH 7.0) for 1.5 h at 24°C. Then, 10 mM of preassembled F-actin were incubated with 0.35 μM of $AopW1_{101-485}$, 2 μM α-actinin (positive control,) or 2 μM BSA (negative control) for 1 h at 24°C and centrifuged at 150 000 ***g*** for 1.5 h. Proteins from 20-μl aliquots from pellet or supernatant fractions were separated in a 4–20% SDS-PAGE gel and stained with Coomassie blue solution (Fermentas). Relative quantification of actin in gels was done with ImageJ. To check the presence of $AopW1_{101-485}$ in the supernatant fraction, Western blots were performed using His-Tag monoclonal antibodies.

Agrobacterium-mediated transient expression on *N. benthamiana* leaves and assessment of subcellular localization

For *Agrobacterium*-mediated transient expression, the *aopW1* ORFs of strains M6 and 7a1 were amplified with appropriate primers. The resulting products were cloned into pDONR207 entry vector and then mobilized into pEarlyGate 101 binary vector (Earley et al., 2006) by the Gateway cloning system (Thermo Fisher Scientific). The generated plasmids were then transformed into *A. tumefaciens* GV3101 by heat shock transformation as described (Zhou et al., 2009). Transient expression experiments were carried out as described by Roden et al. (2004) with some modifications. Briefly, overnight cultures of *A. tumefaciens* GV3101 carrying the different plasmids were washed with a 10 mM $MgCl_2$ solution, centrifuged at 3500 ***g*** for 5 min, and resuspended in induction

solution containing 10 mM $MgCl_2$, 200 mM acetosyringone, and 10 mM 2-(*N*-morpholino)-ethanesulfonic acid (pH 5.6). The suspensions were then incubated at 25°C without shaking for 3 h. Bacterial cultures were diluted to OD_{600} of 0.6 and infiltrated with a needleless syringe into the abaxial part of leaves of 4-week-old *N. benthamiana* plants.

Subcellular localization of AopW1 was assessed 24 h after inoculation with *A. tumefaciens* GV3101 carrying plasmid pEarleyGate 101 with *aopW1* fused in frame with the YFP gene and a HA tag, and when relevant, 48 h after inoculation with the same strain carrying vectors with different plant markers, respectively. The tested markers were: *Discosoma* red fluorescent protein (DsRed) fused in frame with the actin-binding domain 2 (ABD2) (DsRed-ABD2; Voigt, Timmers, Šamaj, Müller, et al., 2005); monomeric red fluorescence protein (mRFP) fused in frame with the ER marker HDEL (mRFP-HDEL; Schoberer et al., 2009); monomeric Cherry Fluorescent Protein (mCherry) fused in frame with the endosome marker Wave33 (RabD2b) (Bar et al., 2013); the endosome marker FYVE fused in frame with DsRed (Voigt, Timmers, Šamaj, Hlavacka, et al., 2005); and the endosome markers Ara7 (RabF2b) and AtEHD1 fused in frame with cyan fluorescent protein (CFP) (Bar, Aharon, et al., 2008; Bar et al., 2013; Lee et al., 2004). Alternatively, samples were stained with 1 mg ml^{-1} DAPI for detection of the plant cell nucleus. Detection with infrared emission was used to locate the chloroplasts. *Agrobacterium tumefaciens* GV3101 derivative strains carrying pEarleyGate 104 and pEarleyGate 100 were used as positive and negative controls, respectively. Functional fluorophores were visualized with Z-stacks images using a SPE confocal microscope (Leica Microsystems). Contrast and intensity for each image were manipulated uniformly using ImageJ software (Schneider et al., 2012). Experiments were carried out at least twice for each effector/marker combination. Expression of AopW1-YFP on *N. benthamiana* leaves was validated by Western blot analysis using an HA primary antibody.

Cell death and ion leakage assays in *N. benthamiana* leaves

For cell death assays, leaves of 4-week-old *N. benthamiana* were transiently transformed with agrobacteria carrying plasmid pEarleyGate 101 with different AopW1 versions and plasmid harboring pBIN19-*Pro35S*:AtEHD1-GFP or pBIN19-*Pro35S*:free-GFP (control). Controls were agrobacteria carrying plasmid pEarleyGate 101 expressing free-YFP. Plants were kept in a greenhouse under long-day conditions (16 h light/8 h dark), at 25°C, and cell death was quantified 72 h post-injection using ImageJ. Ion leakage (conductivity) measurements were performed according to Leibman-Markus et al. (2017). Briefly, leaf discs (0.9-cm diameter) from *N. benthamiana* leaves transformed with the indicated effectors with or without EHD1, were harvested 18 h after transformation and washed with distilled water for 3 h in 50 ml-Falcon tubes. For each sample, five discs were placed in a 10-flask with 1 ml of distilled water, for 48 h with agitation. After incubation, 1.5 ml of distilled water was added to each sample, and conductivity was measured using an Eutech CyberScan CON 510 instrument (Thermo Fisher Scientific).

Detection of callose deposition in *N. benthamiana* leaves

Callose deposition assays were carried out by the procedure described by Nguyen et al. (2010), with some modifications. Briefly, *N. benthamiana* leaves were infiltrated with 40 μM flg22 (Felix et al., 1999) with a needleless syringe. After 24 h, treated leaves were agroinfiltrated with *A. tumefaciens* GV3101 strain carrying pEarleyGate 101 vector, either empty or containing *aopW1* fused to the YFP gene (OD_{600} adjusted to 0.6). After 24 h, 1-cm diameter disks were collected and serially incubated in 95, 70, and 50% ethanol solutions, for 6, 1,2 and 2 h, respectively, at 37°C with shaking. The ethanol solutions were replaced several times. Then, disks were washed with DDW and stained for 2 h with 1% aniline blue in 150 mM K_2HPO_4 (pH 9.5). Disks were then transferred to a slide containing 60% glycerol in PBS, and callose deposits were visualized using a SPE confocal microscope using 405 nm laser for aniline blue excitation and a 475–525 nm band-pass emission filter for aniline blue fluorescence collection. Contrast and intensity for each image were manipulated uniformly using ImageJ and deposits were counted from six areas from three different leaves from three plants (54 total areas per experiment).

Cell death and ethylene biosynthesis assays in *N. tabacum* leaves

Cell death assays were carried out on 5–6-week-old *N. tabacum* cv. Samsun NN and analyzed as described above for *N. benthamiana*. Leaves were transiently transformed with agrobacteria harboring group I or II AopW1 in combination with pBIN19-*Pro35S*:AtEHD1-GFP or the control plasmid expressing free-GFP, pBIN19-*Pro35S*:free-GFP. In some experiments, agrobacteria harboring pBIN19-*Pro35S*:TvEIX were used. Controls were agrobacteria carrying plasmid pEarleyGate 101 expressing free-YFP. Cell death was quantified 72 h post-injection using ImageJ. Ethylene biosynthesis was measured as previously described (Leibman-Markus et al., 2017). Briefly, leaf disks (0.9-cm diameter) were taken from EHD1-GFP transiently expressing *N. tabacum* plants (same construct as described above), 40 h post-injection. Free-GFP (empty vector) was injected as mock. Five disks were sealed in each 10 ml flask containing 1 ml assay medium (with or without 1 μg ml^{-1} EIX) and incubated with shaking for 4 h at room temperature. Ethylene production was measured by Gas chromatography (Varian 3350; Varian, Palo Alto, CA, USA). For both assays, plants were kept in a greenhouse under long-day conditions (16 h light/8 h dark), at 25°C.

Generation of *A. citrulli aopW1* knockout mutants and complemented strains

Mutant strains impaired in *aopW1* were created in the background of the group I strain M6 and the group II strain 7a1. Briefly, an internal fragment of the *aopW1* ORF (which does not span the 3′ and 5′ends of this gene) was PCR-amplified with suitable primers (Table S4) using DNA from strain M6. The PCR products were cloned into pTZ57R/T, verified by sequencing, excised with appropriate restriction enzymes (Table S4), and then cloned into pJP5603 to yield pJP5603_*aopW1*int (M6). Insertional mutagenesis of the target gene in strains M6 and 7a1 was performed by electroporation, to yield mutants M6-A^- and 7a1-A^-. Gene disruption was confirmed by PCR analyses. For complementation of the mutants, the *aopW1* ORFs of M6 and 7a1 were PCR-amplified along with a 500-bp region upstream of the start codon, in order to include the native promoter of the genes. For this purpose, suitable primers were designed based on the sequence of strain M6. The PCR product was cut with restriction enzymes as detailed in Table S4, and cloned into the broad host vector pBBR-MCS-5. The resulting complementation vectors, pBBR-MCS-5::*aopW1* (M6) and pBBR-MCS-5::*aopW1* (7a1) (Table S2) were verified by sequencing and introduced into mutants M6-A^- and 7a1-A^- by electroporation as described (Bahar et al., 2009). Complemented strains were selected by Gm resistance and confirmed by PCR.

Virulence assays of *A. citrulli* strains on melon and watermelon

Acidovorax citrulli strains were steaked and cultured from −80°C on NA plates with appropriate antibiotics and incubated at 28°C. Bacteria were collected with a solution containing 10 mM $MgCl_2$ and 0.02% silwet L-77 and the suspension was adjusted to an OD_{600} of 0.2 (about 10^8 CFU ml^{-1}) using a spectrophotometer. These suspensions were used to spray-inoculate upper and lower parts of the first two true leaves of 3-week-old melon and watermelon plants until run-off. Plants were covered with plastic bags for 24 h to promote infection and were maintained in a greenhouse at 27°C for 3 dpi for plants inoculated with M6 and derivative strains, or 5 dpi for plants inoculated with 7a1 and derivative strains. The first true leaves from each plant were used to take images for measurement of lesion areas and assessment of *A. citrulli* concentrations in inoculated leaves.

Measurements of lesion area and calculation of percentage of symptomatic area relative to the whole leaf were carried out with ImageJ as described (Tuang et al., 2020) with a total of five leaves per treatment per experiment. Bacterial concentrations in the leaves were estimated at the inoculation time (time 0) and at 3 or 5 dpi (for M6 and 7a1 derivative strains, respectively) by colony counting following serial dilutions of leaf samples in 10 mM $MgCl_2$ (five leaf samples per treatment and time point). Each leaf sample consisted of five 0.5-cm diameter leaf disks that were collected with a puncher and homogenized in 1.5-ml tubes containing 500 µl of 10 mM $MgCl_2$. Serial dilutions were plated on NA with appropriate antibiotics. The plates were incubated for 48 h at 28°C, and the colonies were counted. For ion leakage (conductivity) measurements, leaf disks (five per treatment) were collected at 3 or 5 dpi from the second true leaves, with a 1-cm diameter puncher. They were then washed three times with 3 ml double distilled water (DDW) and kept in 3 ml DDW at room temperature for 3 h. Then, the DDW was removed and 2 ml of fresh DDW were added. Samples were agitated at 250 rpm for 48 h. Then, 1 ml of DDW was added to each sample, and the conductivity was measured using an S30 SevenEasy Conductivity apparatus (Mettler Toledo, Greifensee, Switzerland). These experiments were carried out three times with similar results.

Statistical analysis

The following statistical tests were done with Prism 8 (GraphPad, La Jolla, CA, USA) or JMP software (SAS Institute, Inc., Cary, NC, USA) Student's t-test (two groups, parametric, equal variance), Mann–Whitney test (two groups, non-parametric), one-way ANOVA with Tukey's post hoc test (three or more groups, parametric, equal variance), Kruskal Wallis one-way ANOVA (three or more groups, non-parametric, equal variance) and one-way ANOVA with Dunnett post hoc test (three or more groups, parametric, unequal variance).

AUTHOR CONTRIBUTIONS

SB, IJ-G, FP-M, and MB designed the experiments. IJ-G performed most of the research. MS and NE-L generated some of the constructs and performed some of the experiments with yeast. GMdS, FP-M, and ML-M assisted with co-localization experiments. RG and ZKT carried out some of the experiments involving tobacco, melon, and watermelon plants. LN-G carried out phylogenetic analyses. SB, IJ-G, FP-M, and MB wrote the manuscript.

ACKNOWLEDGEMENTS

This work was supported by research grant IS-5023-17C from the United States-Israel Binational Agriculture Research and Development (BARD) Fund. FP-M was recipient of the José Castillejo grant from the Ministry of Education, Culture and Sport of the Spanish Government and the VI PPIT-US grant from the University of Seville. GMdS was recipient of a Lady Davis post-doctoral fellowship. ZKT was recipient of a Valazzi Pikovsky post-doctoral fellowship. We thank Dr. Joanna Jelenska and Prof. Jean T. Greenberg for kindly providing the pBAV154-dexHopW1-HA plasmid that served as template for amplification of the *P. syringae hopW1* ORF, and Dr. Johannes Sikorski for providing genomic DNA of *X. translucens* pv. *translucens* DSM 18974 that was used for amplification of the ORF of the *hopW1* homolog of this strain. We also thank Prof. Nahum Shpigel for his advice regarding actin staining in yeast, and Dr. Einat Zelinger for the help provided in microscopy techniques.

CONFLICT OF INTEREST

The authors declare that they have no competing interests.

SUPPORTING INFORMATION

Additional Supporting Information may be found in the online version of this article.

Figure S1. Immunodetection of AopW1 variantsin yeast.

Figure S2. Group I AopW1 disrupts actin filaments in yeast.

Figure S3. Effects of single amino acid substitutions in the AopW1 HVR on yeast growth inhibition.

Figure S4. Effects of swap substitutions in position 319 of AopW1 on yeast growth inhibition.

Figure S5. Immunodetection of wild-type and mutated versions of AopW1 expressed in *Nicotiana benthamiana*.

Figure S6. Subcellular localization of the group I (1+2+3) AopW1 variant in *N. benthamiana*.

Figure S7. Subcellular localization of the group II (1+2+3+4) AopW1 variant in *N. benthamiana*.

Figure S8. EHD1 increases defence responses.

Figure S9. Images of melon leaves spray-inoculated with *A. citrulli* M6 and derivative mutants.

Figure S10. Images of watermelon leaves spray-inoculated with *A. citrulli* 7a1 and derivative mutants.

Figure S11. Images of melon leaves spray-inoculated with *A. citrulli* 7a1 and derivative mutants.

Figure S12. Images of watermelon leaves spray-inoculated with *A. citrulli* M6 and derivative mutants.

Figure S13. Conductivity in melon and watermelon leaves spray-inoculated with *A. citrulli* M6, 7a1 and derivative mutants.

Table S1. Yeast growth-inhibition phenotypes induced by different versions of *Acidovorax citrulli* AopW1 and homolog effectors under regular conditions or under stress.

Table S2. Strains and plasmids used in this study.

Table S3. Details of the amino acid residues and positions subjected to site-directed mutagenesis in the HVR of *A. citrulli* M6 (group I) and 7a1 (group II) AopW1.

Table S4. DNA oligonucleotide primers used in this study.

Appendix S1. In silico analysis of the AopW1 chloroplast localization.

REFERENCES

Adams, A.E.M. & **Pringle, J.R.** (1991) Staining of actin with fluorochrome-conjugated phalloidin. *Methods in Enzymology*, **194**, 729–731.

Bahar, O. & **Burdman, S.** (2010) Bacterial fruit blotch: a threat to the cucurbit industry. *Israel Journal of Plant Sciences*, **58**, 19–31.

Bahar, O., **Goffer, T.** & **Burdman, S.** (2009) Type IV pili are required for virulence, twitching motility, and biofilm formation of *Acidovorax citrulli* subsp. *citrulli*. *Molecular Plant-Microbe Interactions*, **22**, 909–920.

Bar, M., **Aharon, M.**, **Benjamin, S.**, **Rotblat, B.**, **Horowitz, M.** & **Avni, A.** (2008) AtEHDs, novel Arabidopsis EH-domain-containing proteins involved in endocytosis. *The Plant Journal*, **55**, 1025–1038.

Bar, M. & **Avni, A.** (2014) Endosomal trafficking and signalling in plant defence responses. *Current Opinion in Plant Biology*, **22**, 86–92.

Bar, M., **Benjamin, S.**, **Horowitz, M.** & **Avni, A.** (2008) AtEHDs in endocytosis. *Plant Signaling & Behavior*, **3**, 1008–1010.

Bar, M., **Leibman, M.**, **Schuster, S.**, **Pitzhadza, H.** & **Avni, A.** (2013) EHD1 functions in endosomal recycling and confers salt tolerance. *PLoS One*, **8**, e54533.

Brachmann, C.B., **Davies, A.**, **Cost, G.J.**, **Caputo, E.**, **Li, J.**, **Hieter, P.** ***et al.*** (1998) Designer deletion strains derived from *Saccharomyces cerevisiae* S288C: a useful set of strains and plasmids for PCR-mediated gene disruption and other applications. *Yeast*, **14**, 115–132.

Burdman, S., **Kots, N.**, **Kritzman, G.** & **Kopelowitz, J.** (2005) Molecular, physiological, and host-range characterization of *Acidovorax avenae* subsp. *citrulli* isolates from watermelon and melon in Israel. *Plant Disease*, **89**, 1339–1347.

Burdman, S. & **Walcott, R.** (2012) *Acidovorax citrulli*: generating basic and applied knowledge to tackle a global threat to the cucurbit industry. *Molecular Plant Pathology*, **13**, 805–815.

Burdman, S. & **Walcott, R.** (2018) *Plant-pathogenic Acidovorax species*. Saint Paul, MN: The American Phytopathological Society.

Cheong, M.S., **Kirik, A.**, **Kim, J.G.**, **Frame, K.**, **Kirik, V.** & **Mudgett, M.B.** (2014) AvrBsT acetylates *Arabidopsis* ACIP1, a protein that associates with microtubules and is required for immunity. *PLoS Pathogens*, **10**, e1003952.

Choi, S., **Jayaraman, J.**, **Segonzac, C.**, **Park, H.J.**, **Park, H.**, **Han, S.W.** ***et al.*** (2017) *Pseudomonas syringae* pv. *actinidiae* type III effectors localized at multiple cellular compartments activate or suppress innate immune responses in *Nicotiana benthamiana*. *Frontiers in Plant Science*, **8**, 2157.

Dean, J.F.D., **Gross, K.C.** & **Anderson, J.D.** (1991) Ethylene biosynthesis-inducing xylanase. *Plant Physiology*, **96**, 571–576.

Earley, K.W., **Haag, J.R.**, **Pontes, O.**, **Opper, K.**, **Juehne, T.**, **Song, K.** ***et al.*** (2006) Gateway-compatible vectors for plant functional genomics and proteomics. *The Plant Journal*, **45**, 616–629.

Eckshtain-Levi, N., **Munitz, T.**, **Zivanovic, M.**, **Traore, S.M.**, **Sproeer, C.**, **Zhao, B.** ***et al.*** (2014) Comparative analysis of type III secreted effector genes reflects divergence of *Acidovorax citrulli* strains into three distinct lineages. *Phytopathology*, **104**, 1152–1162.

Eckshtain-Levi, N., **Shkedy, D.**, **Gershovitz, M.**, **Mateus Da Silva, G.**, **Tamir-Ariel, D.**, **Walcott, R.** ***et al.*** (2016) Insights from the genome sequence of *Acidovorax citrulli* M6, a group I strain of the causal agent of bacterial fruit blotch of cucurbits. *Frontiers in Microbiology*, **7**, 430.

Emanuelsson, O., **Nielsen, H.** & **Von Heijne, G.** (1999) ChloroP, a neural network-based method for predicting chloroplast transit peptides and their cleavage sites. *Protein Science*, **8**, 978–984.

Felix, G., **Duran, J.D.**, **Volko, S.** & **Boller, T.** (1999) Plants have a sensitive perception system for the most conserved domain of bacterial flagellin. *The Plant Journal*, **18**, 265–276.

Feng, F. & **Zhou, J.M.** (2012) Plant-bacterial pathogen interactions mediated by type III effectors. *Current Opinion in Plant Biology*, **15**, 469–476.

Feng, J.J., **Schuenzel, E.L.**, **Li, J.Q.** & **Schaad, N.W.** (2009) Multilocus sequence typing reveals two evolutionary lineages of *Acidovorax avenae* subsp. *citrulli*. *Phytopathology*, **99**, 913–920.

Froger, A. & **Hall, J.E.** (2007) Transformation of plasmid DNA into *E. coli* using the heat shock method. *Journal of Visualized Experiments*, **6**, 253.

Fujiwara, S., **Toshio, M.**, **Nakayama, E.**, **Tanaka, N.** & **Tabuchi, M.** (2022) Host-specific activation of a pathogen effector Aave_4606 from *Acidovorax citrulli*, the causal agent for bacterial fruit blotch. *Biochemical and Biophysical Research Communications*, **616**, 41–48.

Galperin, E., **Benjamin, S.**, **Rapaport, D.**, **Rotem-Yehudar, R.**, **Tolchinsky, S.** & **Horowitz, M.** (2002) EHD3: a protein that resides in recycling tubular and vesicular membrane structures and interacts with EHD1. *Traffic*, **3**, 575–589.

Gietz, D., **Stjean, A.**, **Woods, R.** & **Schiestl, R.** (1992) Improved method for high-efficiency transformation of intact yeast-cells. *Nucleic Acids Research*, **20**, 1425.

Goodin, M.M., **Zaitlin, D.**, **Naidu, R.A.** & **Lommel, S.A.** (2008) *Nicotiana benthamiana*: its history and future as a model for plant–pathogen interactions. *Molecular Plant-Microbe Interactions*, **21**, 1015–1026.

Grant, B.D. & **Caplan, S.** (2008) Mechanisms of EHD/RME-1 protein function in endocytic transport. *Traffic*, **9**, 2043–2052.

Guo, M., **Kim, P.**, **Li, G.**, **Elowsky, C.** & **Alfano, J.R.** (2016) A bacterial effector co-opts calmodulin to target the plant microtubule network. *Cell Host & Microbe*, **19**, 67–78.

Hardham, A.R., **Jones, D.A.** & **Takemoto, D.** (2007) Cytoskeleton and cell wall function in penetration resistance. *Current Opinion in Plant Biology*, **10**, 342–348.

Henty-Ridilla, J.L., **Shimono, M.**, **Li, J.**, **Chang, J.H.**, **Day, B.** & **Staiger, C.J.** (2013) The plant actin cytoskeleton responds to signals from microbe-associated molecular patterns. *PLoS Pathogens*, **9**, e1003290.

Horton, P., **Park, K.J.**, **Obayashi, T.**, **Fujita, N.**, **Harada, H.**, **Adams-Collier, C.J.** ***et al.*** (2007) WoLF PSORT: protein localization predictor. *Nucleic Acids Research*, **35**, W585–W587.

Iha, H. & **Tsurugi, K.** (1998) Shuttle-vector system for *Saccharomyces cerevisiae* designed to produce C-terminal-Myc-tagged fusion proteins. *BioTechniques*, **25**, 936–938.

Jiménez-Guerrero, I., **Pérez-Montaño, F.**, **Da Silva, G.M.**, **Wagner, N.**, **Shkedy, D.**, **Zhao, M.** ***et al.*** (2020) Show me your secret(ed) weapons: a multifaceted approach reveals a wide arsenal of type III-secreted effectors in the cucurbit pathogenic bacterium *Acidovorax citrulli* and novel effectors in the *Acidovorax* genus. *Molecular Plant Pathology*, **21**, 17–37.

Johnson, K.L., **Minsavage, G.V.**, **Le, T.**, **Jones, J.B.** & **Walcott, R.R.** (2011) Efficacy of a nonpathogenic *Acidovorax citrulli* strain as a biocontrol seed treatment for bacterial fruit blotch of cucurbits. *Plant Disease*, **95**, 697–704.

Jones, J.D. & **Dangl, J.L.** (2006) The plant immune system. *Nature*, **444**, 323–329.

Kang, Y., **Jelenska, J.**, **Cecchini, N.M.**, **Li, Y.**, **Lee, M.W.**, **Kovar, D.R.** ***et al.*** (2014) HopW1 from *Pseudomonas syringae* disrupts the actin cytoskeleton to promote virulence in Arabidopsis. *PLoS Pathogens*, **10**, e1004232.

Kapuscinski, J. & **Skoczylas, B.** (1977) Simple and rapid fluorimetric method for DNA microassay. *Analytical Biochemistry*, **83**, 252–257.

Kuranda, K., **Leberre, V.**, **Sokol, S.**, **Palamarczyk, G.** & **Francois, J.** (2006) Investigating the caffeine effects in the yeast *Saccharomyces cerevisiae* brings new insights into the connection between TOR, PKC and Ras/cAMP signalling pathways. *Molecular Microbiology*, **61**, 1147–1166.

Lee, A.H.Y., **Hurley, B.**, **Felsensteiner, C.**, **Yea, C.**, **Ckurshumova, W.**, **Bartetzko, V.** ***et al.*** (2012) A bacterial acetyltransferase destroys plant microtubule networks and blocks secretion. *PLoS Pathogens*, **8**, e1002523.

Lee, G.J., **Sohn, E.J.**, **Lee, M.H.** & **Hwang, I.** (2004) The *Arabidopsis* Rab5 homologs Rha1 and Ara7 localize to the prevacuolar compartment. *Plant & Cell Physiology*, **45**, 1211–1220.

Lee, M.W., **Jelenska, J.** & **Greenberg, J.T.** (2008) Arabidopsis proteins important for modulating defence responses to *Pseudomonas syringae* that secrete HopW1-1. *The Plant Journal*, **54**, 452–465.

Leibman-Markus, M., **Schuster, S.** & **Avni, A.** (2017) LeEIX2 interactors' analysis and EIX-mediated responses measurement. *Methods in Molecular Biology*, **1578**, 167–172.

Li, J. & **Staiger, C.J.** (2018) Understanding cytoskeletal dynamics during the plant immune response. *Annual Review of Phytopathology*, **56**, 513–533.

Macho, A.P. & **Zipfel, C.** (2015) Targeting of plant pattern recognition receptor-triggered immunity by bacterial type-III secretion system effectors. *Current Opinion in Microbiology*, **23**, 14–22.

Mansfield, J.W. (2009) From bacterial avirulence genes to effector functions via the *hrp* delivery system: an overview of 25 years of progress in our understanding of plant innate immunity. *Molecular Plant Pathology*, **10**, 721–734.

Mishra, M., **Huang, J.** & **Balasubramanian, M.K.** (2014) The yeast actin cytoskeleton. *FEMS Microbiology Reviews*, **38**, 213–227.

Mudgett, B.M. (2005) New insights to the function of phytopathogenic bacterial type III effectors in plants. *Annual Review of Plant Biology*, **56**, 509–531.

Nguyen, H.P., **Chakravarthy, S.**, **Velásquez, A.C.**, **McLane, H.L.**, **Zeng, L.**, **Nakayashiki, H.** ***et al.*** (2010) Methods to study PAMP-triggered immunity using tomato and *Nicotiana benthamiana*. *Molecular Plant-Microbe Interactions*, **23**, 991–999.

Nomura, H., **Komori, T.**, **Uemura, S.**, **Kanda, Y.**, **Shimotani, K.**, **Nakai, K.** ***et al.*** (2012) Chloroplast-mediated activation of plant immune signalling in Arabidopsis. *Nature Communications*, **3**, 1–11.

Nomura, K., **DebRoy, S.**, **Lee, Y.H.**, **Pumplin, N.**, **Jones, J.** & **He, S.Y.** (2006) A bacterial virulence protein suppresses host innate immunity to cause plant disease. *Science*, **313**, 220–223.

Nomura, K., **Mecey, C.**, **Lee, Y.N.**, **Imboden, L.A.**, **Chang, J.H.** & **He, S.Y.** (2011) Effector-triggered immunity blocks pathogen degradation of an immunity-associated vesicle traffic regulator in Arabidopsis. *Proceedings of the National Academy of Sciences of the United States of America*, **108**, 10774–10779.

Nottensteiner, M., **Zechmann, B.**, **McCollum, C.** & **Hückelhoven, R.** (2018) A barley powdery mildew fungus non-autonomous retrotransposon encodes a peptide that supports penetration success on barley. *Journal of Experimental Botany*, **69**, 3745–3758.

Paez-Garcia, A., **Sparks, J.A.**, **de Bang, L.** & **Blancaflor, E.B.** (2018) Plant actin cytoskeleton: new functions from old scaffold. In: Sahi, V.P. & Baluška, F. (Eds.) *Concepts in cell biology-history and evolution*. Cham, Switzerland: Springer, pp. 103–137.

Pollard, T.D. (2016) Actin and actin-binding proteins. *Cold Spring Harbor Perspectives in Biology*, **8**, a018226.

Pollard, T.D., **Blanchoin, L.** & **Mullins, R.D.** (2000) Molecular mechanisms controlling actin filament dynamics in nonmuscle cells. *Annual Review of Biophysics and Biomolecular Structure*, **29**, 545–576.

Pollard, T.D. & **Borisy, G.G.** (2003) Cellular motility driven by assembly and disassembly of actin filaments. *Cell*, **112**, 453–465.

Rédei, G.P. (2008) *Encyclopedia of genetics, genomics, proteomics and informatics*. Dordrecht, The Netherlands: Springer.

Roden, J.A., **Belt, B.**, **Ross, J.B.**, **Tachibana, T.**, **Vargas, J.** & **Mudgett, M.B.** (2004) A genetic screen to isolate type III effectors translocated into pepper cells during *Xanthomonas* infection. *Proceedings of the National Academy of Sciences of the United States of America*, **101**, 16624–16629.

Ron, M. & **Avni, A.** (2004) The receptor for the fungal elicitor ethylene-inducing xylanase is a member of a resistance-like gene family in tomato. *Plant Cell*, **16**, 1604–1615.

Salomon, D., **Bosis, E.**, **Dar, D.**, **Nachman, I.** & **Sessa, G.** (2012) Expression of *Pseudomonas syringae* type III effectors in yeast under stress conditions reveals that HopX1 attenuates activation of the high osmolarity glycerol MAP kinase pathway. *Microbiology*, **158**, 2859–2869.

Salomon, D., **Dar, D.**, **Sreeramulu, S.** & **Sessa, G.** (2011) Expression of *Xanthomonas campestris* pv. *vesicatoria* type III effectors in yeast affects cell growth and viability. *Molecular Plant-Microbe Interactions*, **24**, 305–314.

Salomon, D. & **Sessa, G.** (2010) Identification of growth inhibition phenotypes induced by expression of bacterial type III effectors in yeast. *Journal of Visualized Experiments*, **37**, 1865.

Schneider, C.A., **Rasband, W.S.** & **Eliceiri, K.W.** (2012) NIH Image to ImageJ: 25 years of image analysis. *Nature Methods*, **9**, 671–675.

Schoberer, J., **Vavra, U.**, **Stadlmann, J.**, **Hawes, C.**, **Mach, L.**, **Steinkellner, H.** ***et al.*** (2009) Arginine/lysine residues in the cytoplasmic tail promote ER export of plant glycosylation enzymes. *Traffic*, **10**, 101–115.

Serrano, I., **Audran, C.** & **Rivas, S.** (2016) Chloroplasts at work during plant innate immunity. *Journal of Experimental Botany*, **67**, 3845–3854.

Shimono, M., **Lu, Y.J.**, **Porter, K.**, **Kvitko, B.H.**, **Henty-Ridilla, J.**, **Creason, A.** ***et al.*** (2016) The *Pseudomonas syringae* type III effector HopG1 induces actin remodeling to promote symptom development and susceptibility during infection. *Plant Physiology*, **171**, 2239–2255.

Siggers, K.A. & **Lesser, C.F.** (2008) The yeast *Saccharomyces cerevisiae*: a versatile model system for the identification and characterization of bacterial virulence proteins. *Cell Host & Microbe*, **4**, 8–15.

Singh, R., **Lee, S.**, **Ortega, L.**, **Ramu, V.S.**, **Senthil-Kumar, M.**, **Blancaflor, E.B.** ***et al.*** (2018) Two chloroplast-localized proteins: atNHR2A and AtNHR2B, contribute to callose deposition during nonhost disease resistance in Arabidopsis. *Molecular Plant-Microbe Interactions*, **31**, 1280–1290.

Sperschneider, J., **Catanzariti, A.M.**, **DeBoer, K.**, **Petre, B.**, **Gardiner, D.M.**, **Singh, K.B.** ***et al.*** (2017) LOCALIZER: subcellular localization prediction of both plant and effector proteins in the plant cell. *Scientific Reports*, **7**, 1–14.

Studier, F.W. & **Moffatt, B.A.** (1986) Use of bacteriophage T7 RNA polymerase to direct selective high-level expression of cloned genes. *Journal of Molecular Biology*, **189**, 113–130.

Tang, D., **Wang, G.** & **Zhou, J.M.** (2017) Receptor kinases in plant-pathogen interactions: more than pattern recognition. *Plant Cell*, **29**, 618–637.

Thomas, C., **Tholl, S.**, **Moes, D.**, **Dieterle, M.**, **Papuga, J.**, **Moreau, F.** ***et al.*** (2009) Actin bundling in plants. *Cell Motility and the Cytoskeleton*, **66**, 940–957.

Traore, S.M., **Eckshtain-Levi, N.**, **Miao, J.**, **Castro Sparks, A.**, **Wang, Z.**, **Wang, K.** ***et al.*** (2019) *Nicotiana* species as surrogate host for studying the pathogenicity of *Acidovorax citrulli*, the causal agent of bacterial fruit blotch of cucurbits. *Molecular Plant Pathology*, **20**, 800–814.

Tuang, Z.K., **Wu, Z.**, **Jin, Y.**, **Wang, Y.**, **Oo, P.P.Z.**, **Zuo, G.** ***et al.*** (2020) *Pst* DC3000 infection alleviates subsequent freezing and heat injury to host plants via a salicylic acid-dependent pathway in Arabidopsis. *Plant, Cell & Environment*, **43**, 801–817.

van den Ent, F. & **Lowe, J.** (2006) RF cloning: a restriction-free method for inserting target genes into plasmids. *Journal of Biochemical and Biophysical Methods*, **67**, 67–74.

Voigt, B., **Timmers, A.C.**, **Šamaj, J.**, **Hlavacka, A.**, **Ueda, T.**, **Preuss, M.** ***et al.*** (2005) Actin-based motility of endosomes is linked to the polar tip growth of root hairs. *European Journal of Cell Biology*, **84**, 609–621.

Voigt, B., **Timmers, A.C.**, **Šamaj, J.**, **Müller, J.**, **Baluška, F.** & **Menzel, D.** (2005) GFP-FABD2 fusion construct allows in vivo visualization of the dynamic actin cytoskeleton in all cells of Arabidopsis seedlings. *European Journal of Cell Biology*, **84**, 595–608.

Voigt, C.A. (2014) Callose-mediated resistance to pathogenic intruders in plant defence-related papillae. *Frontiers in Plant Science*, **5**, 168.

Walcott, R.R., **Fessehaie, A.** & **Castro, A.C.** (2004) Differences in pathogenicity between two genetically distinct groups of *Acidovorax avenae* subsp. *citrulli* on cucurbit hosts. *Journal of Phytopathology*, **152**, 277–285.

Walcott, R.R., **Langston, J.D.B.**, **Sanders, F.H.** & **Gitaitis, R.D.** (2000) Investigating intraspecific variation of *Acidovorax avenae* subsp. *citrulli* using DNA fingerprinting and whole cell fatty acid analysis. *Phytopathology*, **90**, 191–196.

Wang, Y., **Li, X.**, **Fan, B.**, **Zhu, C.** & **Chen, Z.** (2021) Regulation and function of defence-related callose deposition in plants. *International Journal of Molecular Sciences*, **22**, 2393.

Yoon, S., **Liu, Z.C.**, **Eyobo, Y.** & **Orth, K.** (2003) *Yersinia* effector YopJ inhibits yeast MAPK signaling pathways by an evolutionarily conserved mechanism. *The Journal of Biological Chemistry*, **278**, 2131–2135.

Zhang, C., **Mallery, E.**, **Reagan, S.**, **Boyko, V.P.**, **Kotchoni, S.O.** & **Szymanski, D.B.** (2013) The endoplasmic reticulum is a reservoir for WAVE/SCAR regulatory complex signaling in the Arabidopsis leaf. *Plant Physiology*, **162**, 689–706.

Zhang, X., **Yang, Y.**, **Zhao, M.**, **Yang, L.**, **Jiang, J.**, **Walcott, R.** ***et al.*** (2020) *Acidovorax citrulli* type III effector AopP suppresses plant immunity by targeting the watermelon transcription factor WRKY6. *Frontiers in Plant Science*, **11**, 1723.

Zhang, X., **Zhao, M.**, **Jiang, J.**, **Yang, L.**, **Yang, Y.**, **Yang, S.** ***et al.*** (2020) Identification and functional analysis of AopN, an *Acidovorax citrulli* effector that induces programmed cell death in plants. *International Journal of Molecular Sciences*, **21**, 6050.

Zhao, M., **Dutta, B.**, **Luo, X.**, **Burdman, S.** & **Walcott, R.R.** (2020) Genetically distinct *Acidovorax citrulli* strains display cucurbit fruit preference under field conditions. *Phytopathology*, **110**, 973–980.

Zhao, M. & **Walcott, R.** (2018) *Acidovorax citrulli*: history, epidemiology, and management of bacterial fruit blotch of cucurbits. In: Burdman, S. & Walcott, R. (Eds.) *Plant-pathogenic Acidovorax species*. Saint Paul, MN: American Phytopathological Society, pp. 39–57.

Zhou, H., **Morgan, R.L.**, **Guttman, D.S.** & **Ma, W.** (2009) Allelic variants of the *Pseudomonas syringae* type III effector HopZ1 are differentially recognized by plant resistance systems. *Molecular Plant-Microbe Interactions*, **22**, 176–189.